4

Low-Dimensional Group III-V Compound Semiconductor Structures

Nobuhiko P. Kobayashi
University of California Santa Cruz, Santa Cruz, California, U.S.A.
Advanced Studies Laboratories, University of California Santa Cruz and NASA Ames Research Center, Moffett Field, California, U.S.A.
Bio-Info-Nano Research and Development Institute, University of California Santa Cruz and NASA Ames Research Center, Moffett Field, California, U.S.A.

1. Introduction

1.1 Epitaxial Growth

Epitaxial growth of inorganic materials in the form of single-crystal thin films can be viewed as a special case of crystal growth that is essentially a first-order phase transition exhibited by a wide range of single chemical elements and a variety of compounds including insulator, metals, and semiconductors. Epitaxial growth of thin films can also be viewed as a unique case of those among various deposition processes of thin films. Epitaxial growth of thin films requires a combination of stringent crystal growth parameters that need to be dynamically tuned to establish appropriate growth environment. Everlasting quest to raise the level of perfection of single-crystal thin films by understanding and improving epitaxial growth processes has been a scientific subject that has inspired many scientists in the past. An early attempt of constructing a theory of crystal growth from vapor phase, including many essential aspects of crystal growth, treated surface features (e.g., steps and kinks) on a crystal surface in equilibrium with vapor by obtaining the rate of advancement of monomolecular steps as a function of supersaturation in the vapor and mean concentration of kinks in the steps.[1] Influence of dislocations was also analyzed and growth rate of a surface containing dislocations was shown to be proportional to the square of the supersaturation for low supersaturation and to the first power for high supersaturation. Equilibrium structures of steps (e.g., the statistics of kinks in steps) were also studied in terms of surface temperature, binding energy parameters, and crystallographic orientation. Shape and size of a two-dimensional nucleus in unstable equilibrium with a given supersaturation at a given temperature were obtained. Analyses on the temperature dependence of the structure of perfect surfaces (i.e., surfaces free from steps at absolute zero temperature) showed that a perfect surface remains flat until the surface reaches a roughening transition temperature at which the surface undergoes a morphological transition by which the surface becomes rough dramatically.[2] With the view more practical, a unified theory was developed to understand the physics of epitaxial thin films and applied to tailor epitaxial growth conditions to obtain perfect epitaxial thin films of uniform

thickness.[3] The pursuit of superior epitaxial growth will continues to motivate scientists and engineers in a variety of technical fields for the years to come as the growing demand for high-quality single-crystal thin films needs to be met for a wide range of advanced solid-state devices.

Apparently in epitaxial growth, one of the prerequisites that drive ordinary thin film deposition into epitaxial growth is the use of a single-crystal substrate. A single-crystal substrate is characterized by its constituent atoms chemically bonded each other to form a three-dimensional network that can be described by specific translational and rotational crystallographic symmetries with the presence of long-range atomic ordering. When a thin film is epitaxially grown on a single-crystal substrate, the thin film grows as a single-crystal and a common interface is created between the single-crystal epitaxial thin film and the single-crystal substrate. A single-crystal epitaxial thin film exhibits a crystal lattice having a definite crystallographic orientation with respect to that of a single-crystal substrate, in other words, a single-crystal epitaxial thin film has a specific crystallographic registry with a single-crystal substrate. The surface of a single-crystal substrate, a part critically relevant to epitaxial growth, plays a major role in epitaxial growth, in particular, in the early stage of epitaxial growth. Surfaces of semiconductor single-crystal substrates are known to exhibit a variety of superstructures (surface reconstructions) that have translational and rotational symmetry different from those present in the bulk part of a semiconductor single-crystal substrate. Although various types of surface reconstructions are observed on surfaces of semiconductor single-crystal substrates under different epitaxial growth conditions, a semiconductor thin film grown on a semiconductor single-crystal substrate is eventually connected coherently to the single-crystal substrate, forming an atomically seamless interface between the grown single-crystal semiconductor epitaxial thin film and the single-crystal semiconductor substrate.

Epitaxial growth has been reviewed by numerous times and various theories intended to describe different aspects of epitaxial growth were developed. In particular, nucleation processes in the early stage of epitaxial thin film growth were extensively studied.[4,5,6,7,8,9,10,11] Nucleation processes in epitaxial growth of thin films have been viewed as one of the scientific fields where experimental demonstrations and theoretical analyses progress side-by-side because the nucleation process in the early stage of thin film growth is an ideal case where experimental variable can be fairly well controlled. The study of the nucleation processes led us to recognize the importance of surfaces in the context of epitaxial growth of thin films. Based on thermodynamics, physical properties of, for instance, equilibrium surfaces can be deduced from the knowledge of the free energy associate with equilibrium surfaces. While a surface viewed as the interface between the surface of an epitaxial thin film and surrounding (e.g., vapor phase established in given epitaxial growth environment) is important for the nucleation in epitaxial growth of thin films, the interface between an epitaxial thin film and a substrate or between an epitaxial thin film and another epitaxial thin film is equally critical. The energy associated with the interface between an epitaxial thin film (or multiple epitaxial thin films) and a substrate is of great importance, in particular, when the thin film is made of a material different from that of the substrate. Further understanding of epitaxial growth of thin films in terms of morphological and structural evolution is clearly the goal that can only be attained by continuous efforts in both experimental and theoretical advancement.

1.2 Heteroepitaxial Growth

Among a wide range of material systems that can be obtained by epitaxial growth (i.e., a single-crystal thin film on a single-crystal substrate), several unrivaled characteristics exhibited by such material systems as those made of group III-V compound semiconductors are recognized as their flexibility of being assembled into hetero-structures where dissimilar group III-V compound semiconductors with various chemical compositions are coupled in the form of multiple thin films. Sophisticated epitaxial growth techniques such as molecular beam epitaxy (MBE) and metal organic vapor chemical vapor deposition (MOCVD) have been successfully implemented for the growth of group III-V compound semiconductor multiple thin films both at the level of high-volume manufacturing and cutting-edge research environment and widely used for a variety of electronic and optoelectronic devices including hetero-bipolar transistors, light-emitting-diodes, laser diodes, and multi-junction solar cells.

Epitaxial growth of a thin film (or multiple thin films) of various group III-V compound semiconductors or related alloys on a substrate dissimilar to the thin films to be grown (i.e., heteroepitaxial growth), however can be exceptionally complex in contrast to simple epitaxial growth of similar materials (i.e., homoepitaxial growth such as a silicon thin film on a silicon substrate, a germanium thin film on a germanium substrate, and a gallium arsenide thin film on a gallium arsenide substrate). For instance, simple pictures of nucleation processes and evolution processes that work for homoepitaxial growth may no longer be valid for heteroepitaixl growth because new constraints, such as misfit strain associated with two dissimilar materials having different lattice constants or chemical incompatibility, are present in heteroepitaxial growth. When two materials having different lattice constants are connected via a two-dimensional interface, misfit strain needs to be included in the description of heteroepitaxial growth. Epitaxial growth of a single-crystal thin film on a single-crystal substrate with misfit strain would be recognized as one of the most challenging, yet most appealing, in both scientific and engineering subject that needs to be addressed to gain utmost benefits out of this concept technologically very important.

Within thermodynamic framework, the key topic of heteroepitaxial growth of a single-crystal thin film on a single-crystal substrate with mismatch is free energy associated with the interface (i.e., interface free energy) between the thin film and the substrate. A series of early investigations employed an array of dislocations that connected two infinite single-crystals, giving a clear illustration of a very simple model for a heteroepitaxial structure analyzed semi-quantitatively.[12,13] This simple model was further advanced by the establishment of models that dealt with a single dislocation to calculate three types of inter-crystalline boundaries; a boundary due to a difference of atomic spacing, a twist boundary, and a symmetrical tilt boundary[14], and later the model for two crystals having infinite thickness was refined by introducing mismatch as an independent parameter and treating the thin film as a film with finite thickness in contrast to the substrate having infinite thickness, putting an emphasis on epitaxial growth in which a thin film was grown on a thick substrate.[15,16]

From technological perspective, the goal is to find a route by which, for given misfit, an epitaxial thin film can be grown without generating crystallographic defects (e.g., misfit dislocations) detrimental to a targeting application, therefore it is essential to correlate misfit to the generation of misfit dislocations in terms of available growth parameters that can be experimentally tuned. The various concepts and forms of what is called critical thickness for

heteroepitaxial growth with lattice mismatch were derived. Critical thickness for given misfit provides a useful guide in designing an epitaxial growth process as it gives a thickness beyond which the generation of misfit dislocations is substantially accelerated. For instance, the critical thickness for the growth of a Ge_xSi_{1-x} thin film on a Si substrates was evaluated by assuming that the generation of misfit dislocation sets in when the areal strain energy density of the film exceeds the energy density associated with the formation of a screw dislocation (i.e., energy balance) at a distance from the free surface equal to the film thickness.[17] In addition to the energy balance, force balance was also used to predict a critical thickness for $GaAs/GaAs_{0.5}P_{0.5}$ multiple thin films with the motivation to reduce misfit dislocation density by (a) using film thicknesses below those at which misfit dislocations are formed between layers, (b) matching lattice parameters of the substrate to those of the multilayer taken as a whole; and (c) using misfit strain to drive threading dislocations out of samples.[18]

The concept of critical thickness defined for the transition at which a coherent thin film (a film fully strained and without dislocations) turns into an incoherent thin film (i.e., a film with dislocations) was analyzed within the framework of two models, Frenkel-Kontorowa and Volterra models. [19] It was recognized that the epitaxial growth is basically a dynamical process (i.e., a true equilibrium state is not reached during epitaxial growth), thus coherent-incoherent transition essentially driven by free energy gradients and reaching equilibrium is hindered by energy barriers associated with the generation of misfit dislocations. Inherent nature of epitaxial growth occurring on a two-dimensional plane was explicitly analyzed.[20] Dependence of equilibrium configurations of a single-crystal thin film on the strengths of substrate-thin film, thin film-thin film bonds, and the interfacial misfit was examined in two-dimension,[20] in contrast to early analyses based on a one-dimensional model in which misfit was treated along only one crystallographic direction. The analysis postulated that misfits along two different crystallographic orientations may differ from each other and could be accommodated by cross grids of dislocations. A variety of practical cases have been analyzed to predict detrimental influences of misfit on epitaxial growth and a range of practical approaches have been proposed to minimize damaging influences of misfit and to take full advantage of heteroepitaxial growth.[21,22,23,24,25,26]

In addition to numerous attempts to describe epitaxial growth of thin films within the framework of equilibrium structures, approaches with atomistic view (i.e., *ab initio* calculations) have been also comprehensively investigated. Phenomenological models such as Frenkel-Kontorowa and Volterra models gave intuitive physical pictures, which was the main advantage; while the *ab initio* calculations were developed with the goal of obtaining, for instance interface energy more quantitatively accurately. Early atomistic approaches were used to directly calculate interface energy. [27,28,29] For group III-V compound semiconductors characterized by fairly strong covalent chemical bonds, however substantial discrepancies between outcomes of equilibrium approaches and those obtained from experiments were often noticed due partly to relatively high Peierls barriers. The important role of thermal fluctuations and the influence of free energy gradients were suggested[30] and the dynamics of misfit dislocations relieved by continuous plastic deformation was described.[31] The model, referred to as configuration-dependent reactive incorporation (CDRI) model,[32.33.34] with an atomistic view for the epitaxial growth of group III-V compound semiconductor thin films was developed [37]through kinetic Monte-Carlo simulations and introduced with inspiration of several pioneering experimental works[35,36]

on the nature of the adsorption, dissociative reaction, and incorporation of arsenic molecules in homoepitaxial growth of gallium arsenide and related alloys. The CDRI model accounts for a range of surface kinetic processes such as[37] sticking coefficients of the group III atoms, adsorption coefficients for the group V molecular species, intra-planar migration of group III atoms, inter-planar migration of the group III atoms, the group III local configuration dependent reaction rates for the dissociative molecular reaction of physisorbed group V diatomic molecules, the associative reaction of chemisorbed group V atoms to form diatomic molecules and its subsequent desorption.

Epitaxial growth of thin films (quasi two-dimensional), serving as a basic building block, predominate most of electronic and optoelectronic devices commercially available. In contrast to epitaxial thin films, low-dimensional epitaxial structures, such as semiconductor three-dimensional (3D) islands (quasi zero-dimensional) and semiconductor nanowires (quasi one-dimensional), have opened a new paradigm for group III-V compound semiconductors, emerging as nanometer-scale low-dimensional structures. A range of coherent epitaxial low-dimensional semiconductor structures have been demonstrated on various substrates/surfaces physically incompatible. In this chapter, the first part will describe indium arsenide (InAs), one of group III-V compound semiconductor binary alloys, grown, by molecular beam epitaxy, into the form of three-dimensional (3D) islands (also referred to as self-assembled quantum dots) on gallium arsenide surfaces. Two-dimensional (i.e., nucleating clusters) to three-dimensional (i.e., 3D islands) morphological transition and size evolution/vertical alignment of InAs 3D islands in a single and multiple stacks will be illustrated. The lateral size and size dispersion are found to first increase drastically with a small amount of additional InAs deposition and then decrease and saturate, indicating the onset of a natural tendency for lateral size equalization. The vertical alignment of multiple stacks of 3D islands is a result of strain field generated by InAs 3D islands embedded within a GaAs matrix.

In the second part, indium phosphide (InP), another group III-V compound semiconductor binary ally, nanowires grown by metal organic chemical vapor deposition on non-single-crystal surfaces are described. Unlike conventional epitaxial growth of thin films, the proposed route for growing nanowires requires no single-crystal surface. In principle, only short-range atomic order, in contrast to long-range atomic order required for epitaxial growth of thin film, is necessary for nanowires. A template layer that possesses short-range atomic order prepared on a non-single-crystal surface is employed. Ensembles of InP nanowires grown on a template prepared on a non-single-crystal surface are found to be single-crystal and electrically/optically active, which unlocks attractive applications where III–V compound semiconductors are functionally integrated onto various incompatible material platforms.

2. Indium Arsenide Three-dimensional Islands

2.1 Background

In a wide range of epitaxial growth of thin films, a thin film evolves by undergoing three major stages; nucleation of small nuclei (monolayer and double-monolayer islands, etc.), growth of nuclei, and coalescence of nuclei.[38] Presence of misalignment of nuclei caused by the rotation of nuclei around their axis perpendicular to the surface on which nucleation progressed was a popular subject examined and discussed comprehensively within the

scope of epitaxial growth of thin films, which suggested that misfit dislocations generated in a nucleus change misfit strain within the nucleus.[39] Stability of small nuclei seen in the nucleation stage was studied in terms of their size, misfit, stiffness, and strength of film-substrate interaction, which led conclusions that strain energy associated with both crystallographic registry and misfit promotes three-dimensional growth (i.e., the formation of three-dimensional islands) when the misfit is large.[40] Analysis of equilibrium configurations of growing epitaxial islands was also carried out by considering discrete characteristics of consecutive layers of a growing epitaxial three-dimensional (3D) island and interaction between them.[41] The aim of studying epitaxial growth of 3D islands under equilibrium is to find mutual dependence among various physical aspects involved in the epitaxial growth of 3D islands resulted from layered growth within the islands. Such physical aspects includes, for instance, the number of atomic layers consisting of an island, the number of atoms contained in each layer, chemical bonding within and between layers, substrate interfacial bonding, natural misfit and number of misfit dislocations, over-all strain in an 3D island, the conditions required for stable coherent configurations, etc. For given misfit between an overgrowth and a substrate, the misfit may not be entirely accommodated by an integral number of identical misfit dislocations. Thus, the remaining misfit is accommodated by residual elastic strain within 3D islands. Ultimate goal is to form coherent 3D islands by engineering misfit strain with accurate and reproducible growth conditions.

With highly-sophisticated controllability of every aspect of epitaxial growth conditions provided by, for instance, molecular beam epitaxy and metal organic chemical vapor deposition, epitaxial growth of group IV elemental and group III-V compound semiconductors on lattice-mismatched substrates (i.e., strained epitaxial growth) has been employed as a technique to demonstrate semiconductor 3D islands (also referred to as quantum dots) with nanometer-scale size. Such 3D islands have been extensively studied with the hope of developing further advanced electronic and optoelectronic solid-state devices. The formation of 3D islands is in principal driven by a specific mechanism by which given misfit strain is accommodated by morphological change accompanying with or without plastic deformation. The level of understanding physical pictures of epitaxial growth of 3D islands does not seem to have reached its completion even though enormous efforts have been made in both experimental and theoretical studies.

Epitaxial growth of thin films, in contrast to epitaxial growth of 3D islands, implies that relevant growth processes occur over large area (i.e., size of the area, on a substrate, over which epitaxial growth proceeds does not have direct influence on the way epitaxial growth of a thin film progresses, in other words, size of the area over which epitaxial growth of a thin film progresses is considered to be infinite). Unlike thin films, 3D islands are characterized as small (lateral size ~several tenths of nanometers, and height ~several nanometers) isolated three-dimensional structures, each of which is connected to the surface of a substrate through very small area comparable to its lateral size as in Fig. 1.[42] Semiconductor 3D islands, at least those drawing significant attention with the hope of superior optoelectronic devices in the last decade, are expected to exhibit unique physical characteristics associated with their unique features such as shape, size and electronic structures. Among various semiconductor 3D islands, two material systems; silicon/germanium grown on silicon surfaces and indium arsenide (InAs) grown on gallium

arsenide (GaAs) surfaces have been used as convenient vehicles for extensive study because of their inherent simplicity (e.g., chemical composition).

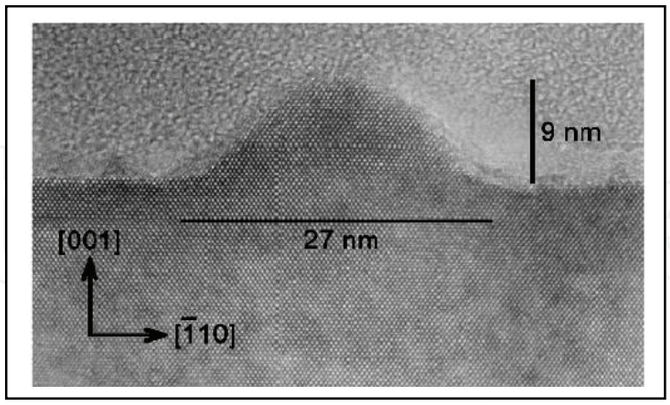

Fig. 1. Lattice image of InAs 3D island obtained by [110] cross-sectional transmission electron microscope lattice imaging. The width and height of the island are 27 and 9 nm, respectively.[42]

Comprehensive reviews in the field of 3D islands (also referred to as quantum dots) are available.[43] In the following section, a series of studies on InAs 3D islands grow on GaAs substrates are described by focusing on three topics; two-dimensional to three-dimensional morphological transition, lateral size equalization, and vertical alignment of an ensemble of 3D islands, all of which are crucially important issues that need to be addressed in the course of implementation of ensembles of 3D islands as a part of solid-state devices.

2.2 Two-dimensional to Three-dimensional Morphological Transition

Formation of coherent 3D islands driven by lattice mismatch between an overgrowth and a substrate has been a fundamental area of research both experimental and theoretical in the field of epitaxial growth in nanometer-scale represented by numerous examples, in particular, with semiconductors such as Ge/Si[44,45] and In(Ga)As/GaAs material systems.[46,47,48,49,50,51,52,53,54,55,56,57] The main focus is to understand the nature of surfaces changing from two-dimensional morphology (i.e., continuous thin films or low-profile, one- or two-monolayer height, two-dimensional clusters appearing in the early stage of highly strained epitaxial growth) to three-dimensional morphology (i.e., surfaces with 3D islands). From solid-state device perspective, early reports on laser oscillation[58,59] from devices that employed InGaAs 3D islands embedded in a GaAs matrix led further studies to clearly correlate optical characteristics of ensembles of 3D islands and lasing characteristics. InAs/GaAs(001) material system has been a vehicle to further understand the atomistic nature of two-dimensional cluster (1ML high) to three-dimensional island (typically 2~4 nm high) transition.

The level of understanding atomistic nature of the two-dimensional to three-dimensional (2D-3D) morphological transition observed in highly-mismatched heteroepitaxial growth has certainly improved dramatically in the past ten years. For many years, the 2D-3D morphological transition was believed to be associated with the formation of defects such as dislocations. However, experimental demonstrations with two semiconductor systems; InGaAs grown on GaAs and Ge on Si, clearly showed that the formation of coherent 3D

islands (i.e., 3D islands without structural defects) is possible in the 2D-3D morphological transition, which has led extensive studies aiming at better atomistic and kinetic understanding of the 2D-3D morphological transition.[33,49,51,52,53,60,61] Therefore, reviewing some of early studies on the 2D-3D morphological transition is worth to acknowledge how much the understanding has advanced. The growth mode characterized by the 2D-3D morphological transition is classically referred to as the Stranski-Krastanow growth mode; however there is clear evidence that the 2D-3D morphological transition in highly-mismatched epitaxial growth is much more complex than the spontaneous change from 2D to 3D morphology described in the framework of the Stranski-Krastanow growth mode.

In the following section, a series of systematic studies on InAs three-dimensional (3D) islands grown on GaAs(001) surfaces by molecular beam epitaxy (MBE) are described. *In situ* ultrahigh vacuum (UHV) scanning tunneling microscope combined with atomic force microscope (STM/AFM) and *ex situ* photoluminescence (PL) and photoluminescence excitation (PLE) were used to study the growth of InAs 3D islands. The amount of InAs delivered onto the GaAs(001) surfaces was varied within the range that covered sub-monolayer to well-formed 3D islands prior to the onset of island coalescence to investigate the initial formation and the subsequent evolution of InAs 3D islands. The details of the sample preparation are as follows and also described elsewhere. [51,62] All samples were grown by MBE on silicon doped n+-GaAs substrates with orientation of (001) ± 0.1 degrees. The growth was monitored by reflection high energy electron diffraction (RHEED). The deposition rate of InAs was calibrated by RHEED on a InAs(001) substrate and determined to be 0.22 ML/s at the substrate temperature of 500 °C and with arsenic beam equivalent pressure of $6x10^{-6}$ Torr. InAs was deposited at 500 °C on a 500 nm GaAs buffer layer that showed clear *c*(4x4) surface reconstruction. The amount of InAs deposition given with respect to the GaAs(001) surface atomic density was confirmed to be reproducible within 0.022 ML. On *in situ* RHEED observation, weak spots superposed on faint streaks appeared at 1.57 ML of InAs coverage, indicating the onset of InAs 3D island formation. All samples were cooled down immediately after the deposition of InAs by shutting off electrical power to the substrate heater in order to minimize post-growth evolution of the grown surfaces so that the nature of InAs 3D island evolution as close as possible to the growth conditions was examined. No intentional annealing or growth interruptions was conducted as these post-growth thermal processes are known to promote a variety of post-growth evolution on grown surfaces.[63,64] The morphological instabilities such as mounds were reported on samples grown with growth interruption[65], which needed to be avoided as much as possible because the formation of 3D islands is extremely sensitive to underlying surface morphology. For instance, diffusion of species on a rough surface can be highly anisotropic.[66] Samples were transferred to the UHV STM/AFM chamber through the UHV interconnect for *in situ* surface characterization. Samples used for *ex situ* PL and PLE were grown on semi-insulating GaAs substrates by following exactly the same procedure described above for the STM/AFM samples with one exception that they were capped with a GaAs thin film grown by migration enhance epitaxy at the substrate temperature of 400 °C.[67]

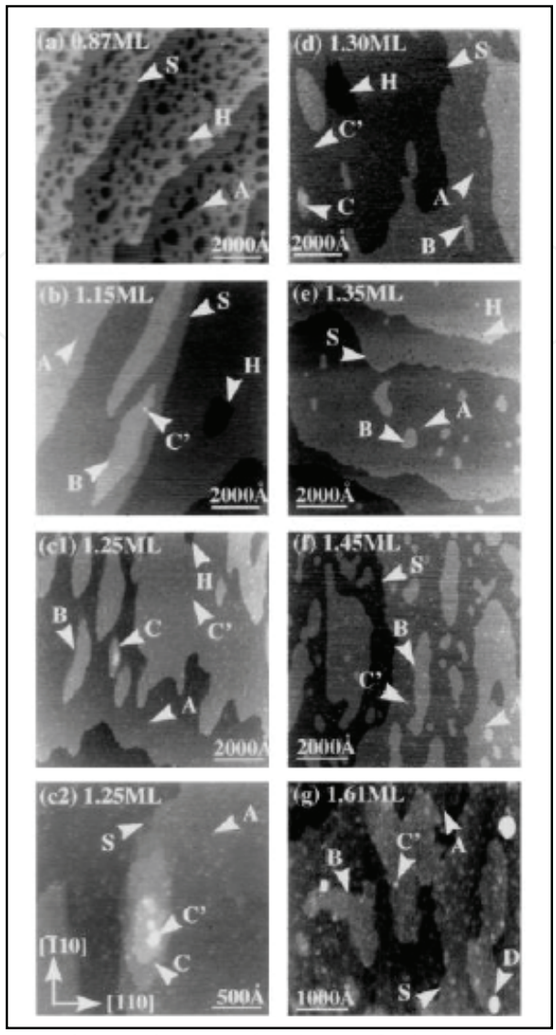

Fig. 2. STM images showing the evolution of InAs on GaAs(001) for depositions of (a) 0.87, (b) 1.15, (c1, c2) 1.25, (d) 1.30, (e) 1.35, (f) 1.45, and (g) 1.61 ML. The labels in the figure denote small 2D clusters (A), large 2D clusters (B), small Q3D clusters (C□), large Q3D clusters (C), 3D islands (D), 1 ML high steps (S), and 1 ML deep holes (H).[68]

Fig. 2 shows a series of STM images of samples grown with the amount of InAs deliveries in the range from 0.87 to 1.61 ML.[68] A varieties of surface features are clearly seen on the samples at different amount of InAs deliveries. 1 ML high steps (labeled *S*) with 200~400 nm wide terraces are seen, which is consistent with the GaAs substrates with tilt of approximately 0.1° used for the growth. The first InAs layer seen in panel (a), generally referred to as a wetting layer, appears to be incomplete up to 1.35 ML InAs delivery in panel (e), evidenced by 1 ML deep holes (labeled *H*). At 0.87 ML in panel (a), the holes cover approximately 20% of the surface. Clusters of up to few nm wide, lateral size <20 nm, and 1 ML high with a high density (>10^{11} cm^2), referred to as *small 2D clusters* (labeled *A*) are seen. Additional InAs delivery, as seen in panel (b), leads to the formation of 1 ML high clusters with width ≥50 nm and lateral sizes up to hundreds of nm (referred to as *large 2D clusters*

and labeled *B*) on top of the still incomplete wetting layer. These large 2D clusters are elongated in the [1-10] direction as seen in panel (b). At the deposition of 1.15 ML in panel (b), features that are 2-4 ML high with respect to the flat InAs surface and up to 20 nm wide (labeled *C'*), referred to as *small quasi-3D (Q3D) clusters*, start to appear. At 1.25 and 1.30 ML InAs delivery in panels (c1) and (d), in addition to the small Q3D clusters, clusters of height of 2-4 ML with lateral extension ≥50 nm, referred to as *large Q3D clusters* are present (labeled *C*). Furthermore, features consisting of a large Q3D cluster (*C*) topped by a small one (*C'*) up to 5 ML high (i.e., features with an extended base and a narrow top) are seen in panel (c2). A notable finding was that the Q3D clusters (small and large) *disappear* once at 1.35 ML, exhibiting a 2D-like surface. Then, as the InAs delivery is further increased to 1.45 ML, only small Q3D clusters *reappear* at a density 2 orders of magnitude higher well before the first 3D islands (7-14 ML high with a lateral size <25 nm) labeled *D* in panel (g) form at 1.57 ML (the critical delivery denoted Q_c). Between 1.57 and 1.74 ML delivery, 2D clusters, small Q3D clusters, and 3D islands co-exist as shown for 1.61 ML deposition in panel (g). Evolution of the 2D clusters, Q3D clusters, and the 3D islands in terms of their area density as a function of InAs delivery is shown in Fig. 3.[68] The Q3D cluster density evidently indicates the appearance, disappearance, and reappearance of 3D morphological features well in advance of the regime in which well-formed 3D islands form. The presence and behavior of the Q3D clusters play a major role in analyzing PL and PLE studies in the following section.

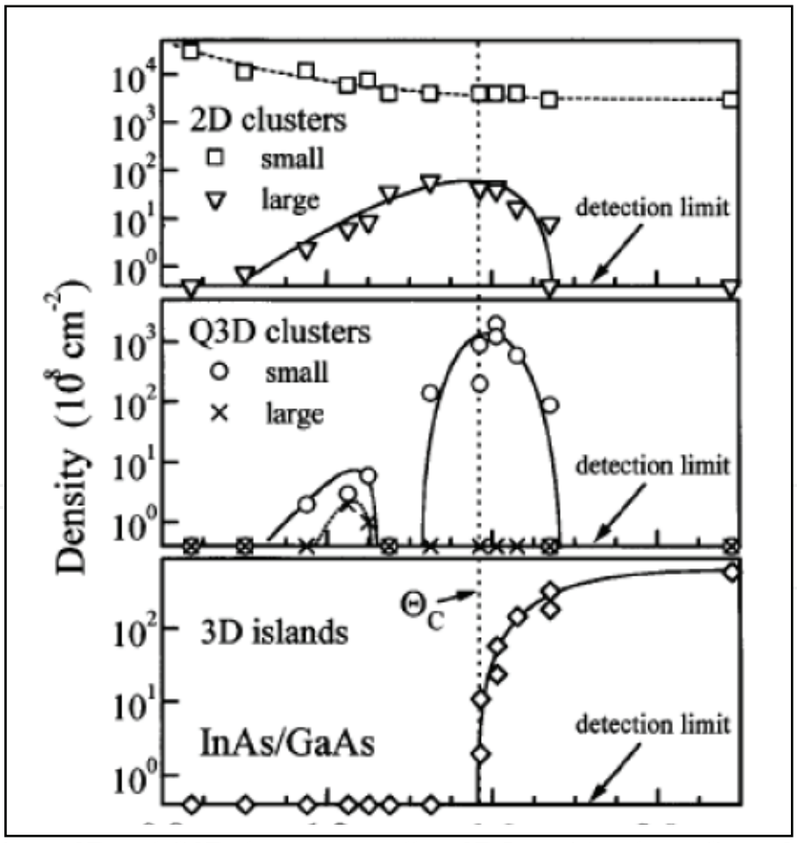

Fig. 3. Area density of 2D and Q3D clusters as well as 3D InAs islands on GaAs(001) as a function of InAs delivery.[68]

Fig. 4 shows the evolution of the PL spectra from 1.00 to 2.00 ML InAs delivery. The narrow peak, attributed to recombination in the wetting-layer, near 1.45 eV evolves with increasing InAs delivery and vanishes just beyond Q_c. The peak at 1.215 eV for the 2.00 ML sample is attributed to recombination in 3D islands as reported earlier.[52,57,69] The PL spectra of the 1.15 and 1.25 ML samples reveal weak, yet distinct, peaks at 1.322 and 1.274 eV, respectively, however, no peak is resolved in the range between 1.20 and 1.35 eV for the 1.35 and 1.45 ML samples. At 1.55 ML delivery (just below Q_c), emission in the range between 1.20 and 1.35 eV reappears, indicating a re-entrant PL behavior showing similarity to that observed in Figs. 2 and 3. The peaks at 1.322 and 1.274 eV in the 1.15 and 1.25 ML samples are attributed to the large 2D and large Q3D clusters serving as parts where the wetting-layer is locally thicker. A comparison with the STM information on the morphology of the InAs layer suggests that *small* Q3D clusters (i.e., feature *C'* in Fig. 2) on top of large 2D and large Q3D clusters act as optically active quantum dots. The observation of emission from the coupled structure of small Q3D clusters on large 2D clusters also explains the disappearance of the PL in the 1.20 to 1.35 eV range for the 1.35 ML sample with no small Q3D clusters, indicating that dominant nonradiative recombination takes place in the large 2D clusters.

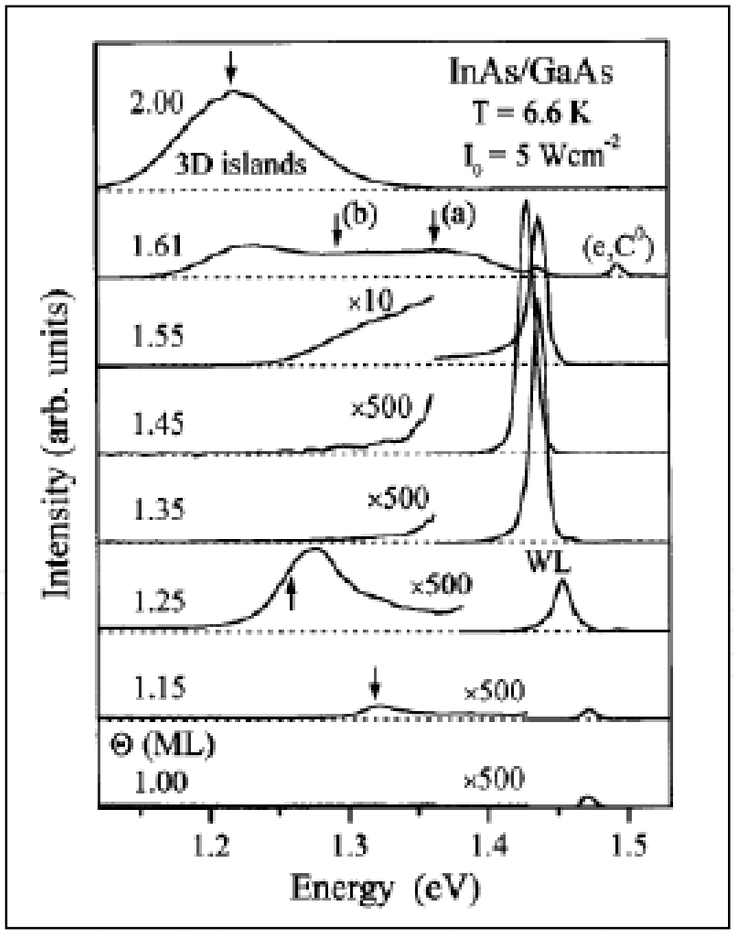

Fig. 4. PL spectra for InAs on GaAs(001) at various depositions Q, excited at 514 nm with a density of 5 Wcm^{-2}. The peak at 1.493 eV (1.61 ML sample) is attributed to carbon-related recombination in the GaAs barrier.[68]

The structural and optical studies on the comparable samples provide a detailed picture of the kinetically controlled evolution of heteroepitaxially grown InAs surfaces. InAs is incorporated in higher layers even before the first InAs layer is completed. In addition to 2D clusters, Q3D clusters form for depositions as low as 1.15 ML due mainly to the strain-driven surface kinetics near the edges of 2D clusters. The strain fields at the edges of 2D clusters lead to an asymmetry in inter-planar In diffusion,[33] promoting the formation of Q3D clusters possible. Therefore, the Q3D features disappear above 1.30 ML because of the change in the surface strain fields when the first InAs ML reaches nearly its complete coverage. The reappearance of the small Q3D clusters with a further increase in In delivery leads to a low energy tail in the wetting-layer peak in Fig. 4 for 1.55 ML. The high density of small Q3D clusters at 1.61 ML, corresponding to an average separation of 22 nm indicates that they act as precursors of 3D islands. It must be emphasized however, that surface morphology of InAs on GaAs(001) material systems near the 2D-3D morphological transition shows a variety of surface features,[53,61,70.71.72] thus a unique picture would need to be established for a series of samples grown under specific growth conditions and schemes. For instance, InAs/GaAs(001) system grown with a growth interruption and studied by atomic force microscope showed that the evolution of 3D islands exhibited two transition onsets at 1.45 and 1.59 ML of InAs coverage, corresponding to the formation of two distinguishable families, small and large islands.[73] The transition between the two families of islands and the explosive nucleation of the large islands seem to be associated with the erosion of step edges around the islands. Furthermore, *in situ* RHEED measurements of the surface evolution during the growth of InAs 3D islands on GaAs showed that InAs 3D islands desorbed when arsenic supply was interrupted.[74]

2.3 Lateral Size Equalization

The formation of three-dimensional (3D) coherent islands in the process of heteroepitaxial growth of material systems with large lattice mismatch and their unique optical properties, demonstrated for InAs 3D islands grown on GaAs,[67,75] have motivated us to find a way to describe mechanisms that govern the formation and evolution of semiconductor 3D islands in the framework of Stranski–Krastanow growth mode. Growth conditions (e.g., the influence of group V pressure, substrate temperature, and growth procedure without or with growth interruption during InAs delivery) employed for the formation of InAs 3D islands have been carefully examined.[52,53,67,75,76,77,78,79] The kinetic processes impacting the evolution of semiconductor 3D islands and their size distribution are two subjects highly relevant to envisioning practical implementation of ensembles of semiconductor 3D islands as an active or a passive part in solid-state devices Therefore, systematic study, using *in situ* ultrahigh vacuum (UHV) atomic force microscope (AFM) and scanning tunneling microscope (STM), on the growth of InAs 3D islands on GaAs(001) surfaces is essential. The unique evolution of InAs 3D islands at sequential growth stages characterized by specific InAs coverage is described in the following section with the aim at minimizing size distribution of an ensemble of InAs 3D islands.

All experiments were carried out in the integrated, ultra-high-vacuum-interconnected, molecular beam epitaxy (MBE) growth-processing-characterization system to conduct growth and analysis without having samples exposed to air. InAs deposition was done at the substrate temperature (T_s) 500 °C with the arsenic beam equivalent pressure (P_{As4}) $6x10^{-6}$ Torr on GaAs(001) surfaces showing *c*(4x4) surface reconstruction ensured by reflection

high-energy electron diffraction (RHEED). The desired amount of InAs (0.87 to ~2.18 ML with respect to the GaAs(001) surface atomic density) was delivered at a growth rate of 0.22 ML/s with an accuracy and precision of ±0.07 ML and ±0.022 ML, respectively. As the In incorporation coefficient is expected to be unity under the growth conditions employed in the experiment, all the delivered InAs is incorporated into the solid. At ~1.57 ML InAs delivery, the RHEED pattern showed weak spots along with faint streaks, signifying the onset of 3D island-like features. The power to the substrate heater was turned off immediately after the deposition of InAs to let T_s drop rapidly. At T_s of 450 °C, P_{As4} was decreased to $1x10^{-6}$ Torr and at T_s of 400 °C the As_4 flux was shut off completely. The above-mentioned growth and cooling procedures were strictly followed for each growth run in order to maintain consistency among all the samples. The unique cooling procedure minimizes and, more importantly, keeps post-growth evolution of the grown surfaces similar from sample to sample. Contact-mode AFM was used to measure density, lateral width and height of InAs 3D islands. To avoid ambiguities in determining the island size dispersion, all island size measurements on a given sample were completed with the same AFM tip. Two different AFM tips were used for the study of our samples and the data obtained using these two tips were found to be consistent with each other. Therefore, while the absolute values of the measured lateral sizes, as is well known in scanning probe microscopy, are an upper bound[80], the relative values within a sample and between samples can be relied upon.

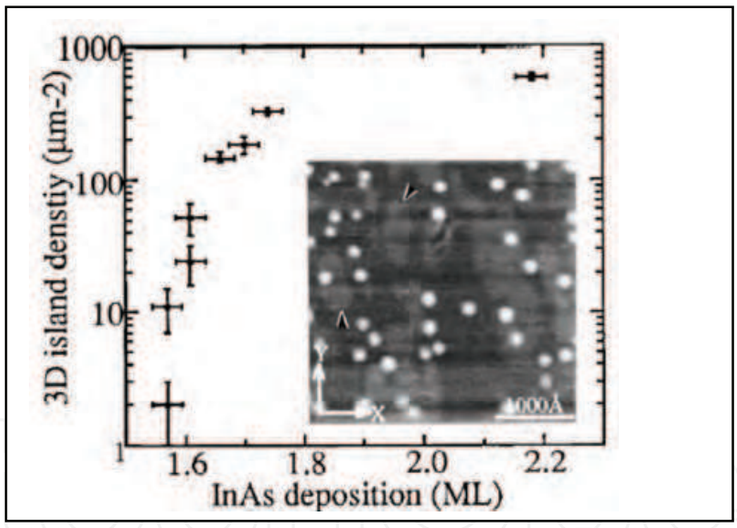

Fig. 5. InAs 3D island density as a function of InAs deposition. The inset shows an *in situ* UHV AFM image for ~1.70 ML InAs deposition on GaAs(001). The bright "spots" are 3D islands while the "patches" in the background (some of these are indicated by arrows) are 2D clusters. The notations X and Y refer to the crystallographic directions [110] and [1 ¯10], respectively.[51]

The AFM image shown as an inset in Fig. 5 is for ~1.70 ML InAs delivery and represents the AFM images obtained for InAs delivery >1.57 ML. The bright spots are the InAs 3D islands. The ''patches'' (marked by two arrow-heads) are 2D clusters with one monolayer high with respect to their surroundings. The areal density of the InAs 3D islands is plotted in Fig. 5, which indicates that the areal density increases rapidly for InAs delivery from 1.57 to 1.74

ML and then slows down from 1.74 to 2.18 ML, reaching a maximum value of ~$6x10^2$ μm^{-2} before island-coalescence begins to set in. Correspondingly, the STM determined that the areal density of the quasi-3D clusters rises to a maximum of ~$2x10^3$ μm^{-2} at 1.61 ML and then drops, reaching near zero for >1.75 ML InAs delivery. The InAs 3D island lateral size and height distributions are plotted in Fig. 6(a) and (b) for different InAs 3D island densities. The lateral size of a 3D island is defined as the full width at half maximum of the island height. As seen in Fig. 6(a), initially when the 3D island density is ~11 μm^{-2} the islands have a narrow lateral size distribution, however as the island density increases to around 24 μm^{-2}, the island lateral size distribution broadens significantly without an evident peak. Concomitantly, the average lateral size seems to increase as well. Remarkably, further increase in island density (~58 μm^{-2}) makes the island lateral size distribution narrow again and the average lateral size also becomes smaller. Thereafter, with increasing island density, the lateral size distribution becomes narrower, while maintaining an essentially constant average lateral size, and then practically invariant as a function of coverage prior to the onset of island coalescence. The evolution of the InAs 3D island height distribution as seen in Fig. 6(b) appears to exhibit the similar but not identical trend to that of the lateral size distribution. Certain variation in the heights is observed at any given island density, which clearly indicates that the islands coexisting at a given evolution stage do not have definite shape (e.g., equilibrium shape), thus their formation is kinetically controlled. It is important to note that the transition from a narrow to a broad and back to a narrow island lateral size distribution under the growth conditions employed in the experiment occurs over a very small increase (<0.08 ML), thus extreme care in the control of deposition amount is required for this notable observation. An initial broadening and subsequent narrowing reported[53,76,77] for near equilibrium islands further suggests that this nature of island evolution is a general phenomenon occurring over the entire range from highly kinetically controlled regime to near thermodynamic equilibrium.

The above remarkable findings in this carefully controlled series of systematic experiments thus not only provide stringent tests for models[33,60,78,81] of strained epitaxy and island formation but also provide insights into the nature of atomistic kinetic processes[33,78] consistent with the observations. The observed initial broadening in the island lateral size distribution and increase in average size up to island density of ~24 μm^{-2} can be understood if, at the earliest stages, the 3D island initiation rate is constant and their growth rates are independent of each other. In this case the size of an island at this stage is simply determined by the time that passes since its initiation provided surface diffusion and incorporation of atoms at the island periphery are not rate limiting steps. The narrowing of the lateral size distribution and the reduction in the average lateral size beyond ~24 μm^{-2} island density in Fig. 6(a) indicate that the above mechanism of island formation at the earliest stage is subsequently replaced by some other evolution mechanism(s) as deposition proceeds. Two important kinetic processes contributing to island growth provide mechanisms consistent with this narrowing. The first is the suggestion based upon thermodynamic energy considerations[33,78,81] that the growth rate of 3D islands would diminish when an island grows to a certain size due to the accumulation of elastic strain energy. From the kinetic viewpoint underlying strained growth simulations,[33] this has been modeled as an attendant increase in an energy barrier for atom incorporation at island edges. As a consequence, at this stage, smaller islands will grow more rapidly, along with the possible formation of new islands. The second contribution is suggested[78] to arise when,

with increasing island density in response to continued InAs delivery, the island-induced strain fields in the substrate (that help to stabilize coherent larger islands in the first place) begin to interact.

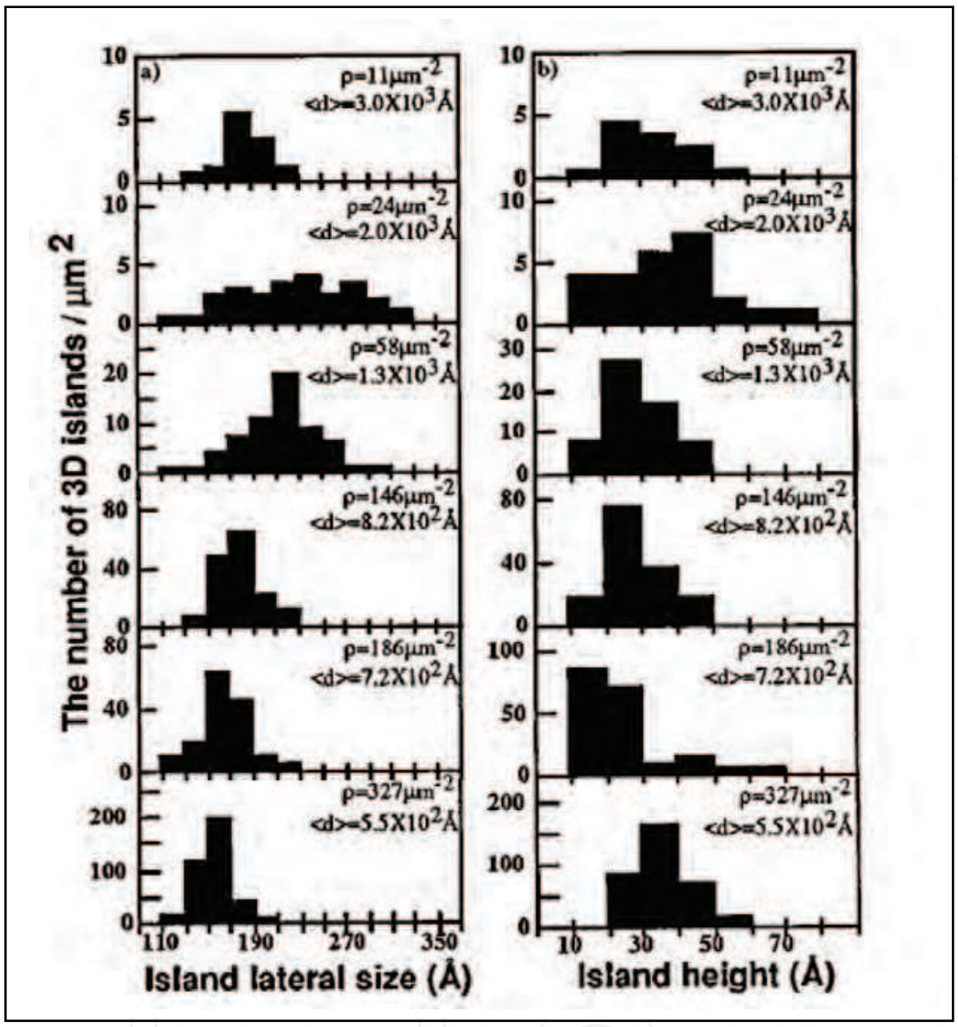

Fig. 6. InAs 3D island (a) lateral size and (b) height distribution for different total InAs 3D island densities, ρ. Also indicated is the mean inter-island separation, $\langle d \rangle = \rho\text{-}1/2$.[51]

At this stage a *driving force* for preferential migration of atoms towards smaller islands can arise due to a downward tilt in the surface potential towards the smaller islands caused by the presence of the interacting island-induced strain fields in the substrate. The interacting strain fields in the substrate and the wetting layer also provide a means to destabilize the initially largest islands by not accommodating as much strain relief in the substrate and thus, from a kinetic viewpoint, decrease the barrier for detachment of atoms from the larger islands. The detachment of atoms from the larger islands can give rise to the loss of material from the initially largest islands, consistent with the AFM results shown in Fig. 6(a) and contributes to island size equalization as well as narrowing of the average size and potentially a change in the island shape. Such *kinetic* processes are likely to begin to impact island growth when the inter-island distance becomes comparable to the range of the

individual island-induced strain fields and a characteristic length, such as the surface diffusion length of the adatoms. The observed value of island density (~24 μm^{-2}) in Fig. 6(a) can be converted to a mean inter-island separation, which results in ~200 nm, the critical inter-island distance, for which the manifestation of island–island interaction is expected to rise rapidly. Indeed, the diffusion length of In during InAs growth on GaAs under the same growth conditions as used in this study has been independently estimated[56] to be ~280 nm, which is comparable to the critical inter-island distance indicated by the AFM studies of the island size evolution behavior described above. The similar trend of narrowing lateral size distribution was reported on double-stacked InAs 3D island on GaAs at island density much higher (~1800 μm^{-2}) than those in our studies[82], indicating that the proposed mechanisms that control overall island lateral size and lateral size distribution are fairly applicable to various InAs 3D islands formed under substantially different growth conditions and/or growth schemes. Various mechanisms that would result in narrow island size distribution have been proposed,[60,83,84] and this subject will continuously be a critical and challenging in the epitaxial growth of semiconductor 3D islands.

2.4 Vertical Alignment

"Stress Engineering" can be referred to as, within the scope of epitaxial growth, the deliberate use of elastic strain naturally or artificially generated within a medium to control kinetics in the process of epitaxial growth. Misfit strain, for instance, can provide a natural driving force for 3D islands in lattice mismatched growth such as InAs on GaAs. Coherent InAs 3D island formation on GaAs(100) offers an bottom-up approach to fabrication of optically efficient 3D islands.[75,85] Given the random initiation of islands on a starting surface of GaAs(100), a certain degree of spatial randomness always sets, resulting in spatial randomness of the locations of 3D islands. In the following section, strain fields induced by 3D islands embedded in a protective cap layer are used, with the spirit of "Stress Engineering", to demonstrate self-organization of InAs 3D islands along the vertical (i.e., growth) direction to examine the potential role of the evolving and interacting strain fields generated within a cap layer by multiple InAs 3D islands.

Molecular beam epitaxy (MBE) was used to grow InAs 3D islands on GaAs(100) substrates.[51] A GaAs buffer layer was grown on a GaAs(100) substrate first, then, the first set of InAs 3D islands were formed at the substrate temperature (T_s) 500 °C with the arsenic beam equivalent pressure (P_{As4}) $6x10^{-6}$ Torr on the GaAs buffer layer showing *c*(4x4) surface reconstruction. Subsequently, the first set of InAs 3D islands were overgrown by a GaAs spacer layer. The thickness of the GaAs spacer layer was varied in the range from 30 ML to 200 ML. The GaAs spacer layer was further followed by the growth of the second set of InAs 3D islands. This combination of the growth of InAs and GaAs spacer was repeated one or more times to obtain two or more sets of islands separated by GaAs spacer layers. Based on RHEED analysis, the growth of InAs on a GaAs spacer layer did not show any apparent differences from the growth of the first set of InAs 3D islands. Transmission electron microscope (TEM) was used to investigate the samples having multiple sets of InAs 3D islands separated by multiple GaAs spacer layers having various thicknesses.

Fig. 7(a) shows a representative [011] cross-sectional TEM (XTEM) picture of a sample with two sets of InAs 3D islands separated by a GaAs spacer of 46 ML. From the strain contrast of the islands in the two sets, each island in the second set is seen to be located on top of another in the first set, which indicates that a strong one-to-one vertical correlation between

the two sets is present. A detailed statistical analysis on the sample reveals that the paring probability of islands in the two sets, measured from XTEM projected images, is 0.885 ± 0.032. The pairing probability drops to 0.492 ± 0.04 when the GaAs spacer thickness increases to 92 ML as in Fig. 7(b).

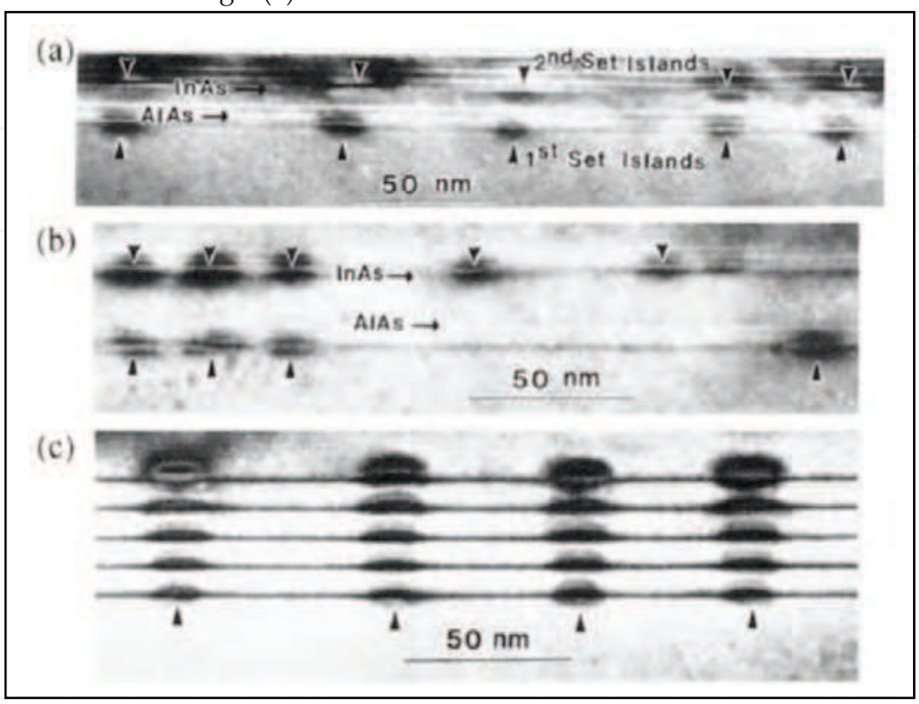

Fig. 7. Typical *g* = (400) bright field TEM pictures taken along [011] azimuth for the samples with two sets of islands separated by (a) 46 and (b) 92 ML spacer layers, respectively. Arrows point to the island positions indicated by the strain contrast. (c) A typical *g*= (200) dark field TEM picture of a sample with five sets of islands separated by 36 ML spacer layers.[56]

For a sample with five sets of islands separated by 36 ML thick spacers grown by migration enhanced epitaxy in Fig. 7(c), the probability of island pairing to the set just below is maintained at approximately ~0.95 for all adjacent island sets. High resolution lattice images confirmed that the spacer layer is atomically flat and the islands are coherent. Possible intermixing between InAs 3D islands and a GaAs spacer layer is an issue that needs to be further addressed since the evidence of intermixing between InAs 3D islands and a GaAs cap layer during the growth of the cap layer and resulting change in shape and composition of InAs 3D islands were reported.[86] Fig. 8 summarizes the pairing probabilities obtained as a function of the spacer thickness using both [011] and [011-] XTEM azimuths. Three distinguishable regimes can be seen; (1) for small spacer thickness <36 ML, the probability is greater than 95%, indicating a nearly completely correlated behavior, (2) a regime of gradual decrease in the probability, and (3) for larger thickness, the probability saturation at a value corresponding to random overlapping of islands. A model analysis accounting for the mechanochemical surface diffusion gives an island average size and average separation dependent characteristic spacer layer thickness below which a vertically self-organized growth occurs.[56] Vertical alignment of InAs 3D islands are also investigated as a means to

improve size distribution. The thickness of a GaAs spacer layer was varied to study its influence on the structural and optical properties of InAs 3D islands. The structural and optical properties of multi-stacked InAs 3D islands grown on GaAs surfaces were studied by photoluminescence measurements. The PL full width at half maximum, reflecting the size distribution of the islands, was found to reach a minimum for an GaAs spacer layer with a thickness of 30 ML.[87] Similar vertical self-organization of InAs 3D islands with GaAs spacer layers was observed in samples grown by metal organic chemical vapor deposition,[88] suggesting this particular "Stress Engineering" is applicable for various epitaxial growth methods.

3. Indium Phosphide Nanowires on Non-single-crystal Surfaces

3.1 Background

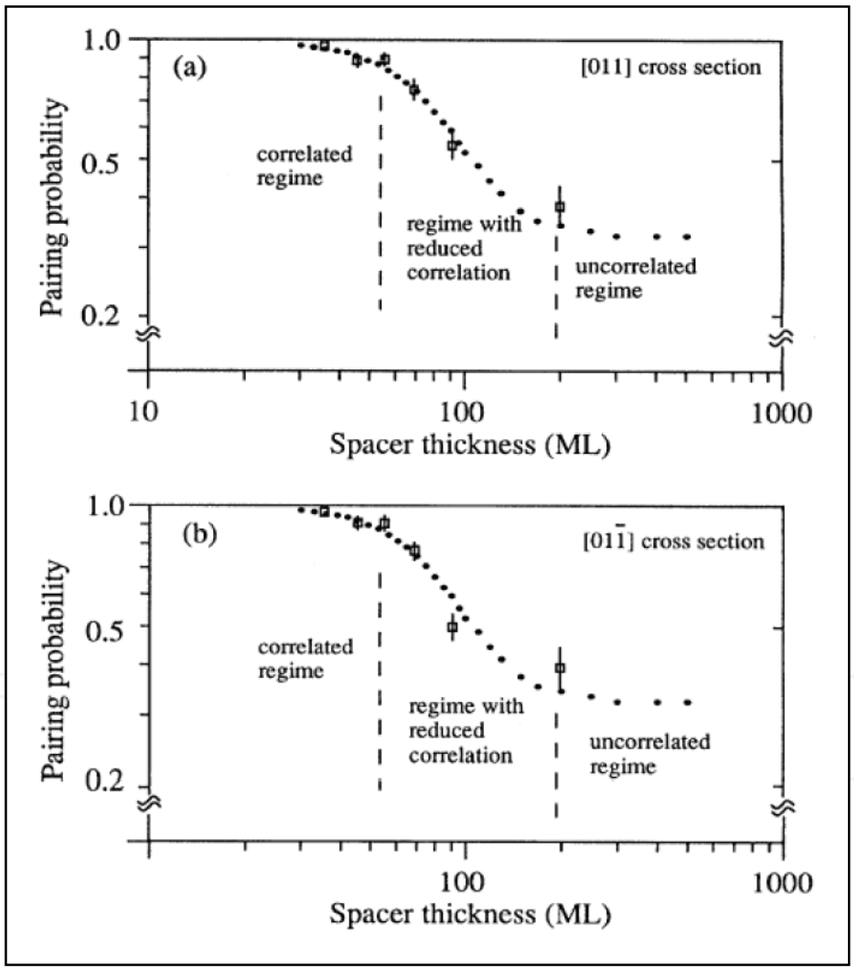

Fig. 8. Experimentally observed paring probabilities (open squares) as a function of the spacer thickness shown on a log-log plot of samples with two sets of islands (a) [011] cross section, and (b) [011-] cross section.[56]

As a natural extension from epitaxial growth of thin films (two-dimensional epitaxial growth), epitaxial growth of three-dimensional (3D) islands (zero-dimensional epitaxial growth) described in the previous section appears to fall into a category of a special case of the formation of thin films accompanying significant morphological transition because of large misfit between a thin film and a substrate. Completely apart from thin films and 3D islands can be seen in the recent surge in the field of one-dimensional epitaxial growth (e.g., semiconductor nanowires). In particular, nanowires of group IV elemental and group III-V compound semiconductors grown with the aid of metal catalyst in the form of nanometer-scale particles are often referred to as vapor-liquid-solid (VLS) growth proposed over forty years ago.[89] Nanowires can be viewed as a structure highly anisotropic in shape with the first and the second dimensions (i.e., diameter in the range of tens of nanometers) much smaller than the third dimension (i.e., length up to several micrometers). In a nanowire, chemical composition can be modulated along its long axis as well as in a concentric manner as seen in Fig. 9(a) and (b), respectively.[90,91] A wide variation in nanowire growth mechanisms that appears to be different from the VLS growth, for instance vapor-solid-solid (VSS) and nanowire growth without metal catalyst, has also been reported.[92,93] The growing number of literatures in this field clearly indicates that various techniques for the growth of nanowires will be continuously developed. Nanowires are expected to exhibit, as seen for semiconductor 3D islands, intriguing physical characteristics strongly associated with their unique electronic structures substantially different from those of bulk and with a large surface to volume ratio, a characteristic totally ignored in bulk. Lateral size (i.e., diameter) of semiconductor nanowires can be comparable to a variety of characteristic lengths such as exciton Bohr radius, electron/hole mean free paths, and electron phase coherence length, etc., thus in nanowires, physical properties related to these characteristics lengths are expected to be strongly influenced by the diameter of nanowires.[94] A nanowire having a large surface to volume ratio implies that the number of atoms existing on the surface of a nanowire is no longer negligible compared to the number of atoms inside of a nanowire, thus the surface of a nanowire is expected to contribute considerably to the ways physical properties are exhibited by a nanowire. For instance, such a bulk property as electrical resistivity cannot be simply defined for a material in the form of nanowire because of the presence of significant contribution from its surface to electrical transport properties. Several comprehensive reviews in the field of nanowires are available.[95] Apparently large surface to volume ratio can be either advantage or disadvantage. Large surface to volume ratio would be very beneficial when solid-state sensors that employ nanowires are envisioned. In contrast, proper handling is required to minimize undesirable physical contributions from large surface area. For instance, nonradiative carrier recombination associated with surface states that scale with total surface area would adversely affect performance of solid-state devices in which photons need to be generated by radiative carrier recombination or photons need to be converted into electrons and holes.

When nanowires are implemented as an active or a passive part of solid-state devices, advantage of using nanowires is recognized as that the volume of a single nanowire is much larger than that of, for instance, a single 3D island. Given such an anisotropic shape, nanowires are of great interest as they are expected to show strong quantum confinement for charged carriers within their cross-section (i.e., within the area defined by their diameter) while charged carriers would move fairly freely along their length. Within the scope of epitaxial growth, in particular heteroepitaxial growth, epitaxial growth of single-crystal

nanowires with diameter significantly smaller than those length-scales relevant to heteroepitaxial growth of thin films offers an opportunity of setting environment where a significant degree of elastic relaxation of misfit strain is expected,[90,96,97,98] which further offers significant advantage when, for instance, heterogeneous integration of nanowires as an optically active part on integrated electronic circuits is envisioned. (e.g., optoelecronic functionalities of group III-V compound semiconductor nanowires integrated on silicon-based electronics). It should be noted, however, the implementation of nanowires as an active part of solid-state devices would not be as straightforward as it appears. Ensembles of quantum dots have been employed as an active part of solid-state devices such as lasers, light-emitting diodes, and photodetectors by simply replacing an active semiconductor thin film by an ensemble of semiconductor quantum dots embedded in a thin film. Nanowires, however, owing to their highly anisotropic shape, non-conventional device designs need to be developed to accommodate one-dimensional shape of nanowires without hampering their unique characteristics. In the following section, our research on group III-V compound semiconductor nanowires is described with strong emphasis on developing a practical yet flexible route to integrate ensembles of nanowires onto various material platforms for a wide range of solid-state devices.

3.2 Ensembles of Nanowires on Non-single Crystal Surfaces

Employing high-quality single-crystal substrates for epitaxial growth is a prevalent practice when high-quality epitaxial films over large-area are required, as a result, significant efforts have been dedicated in developing epitaxial growth processes that produce epitaxial films that are homogeneous in composition and uniform in thicknesses over required areas.

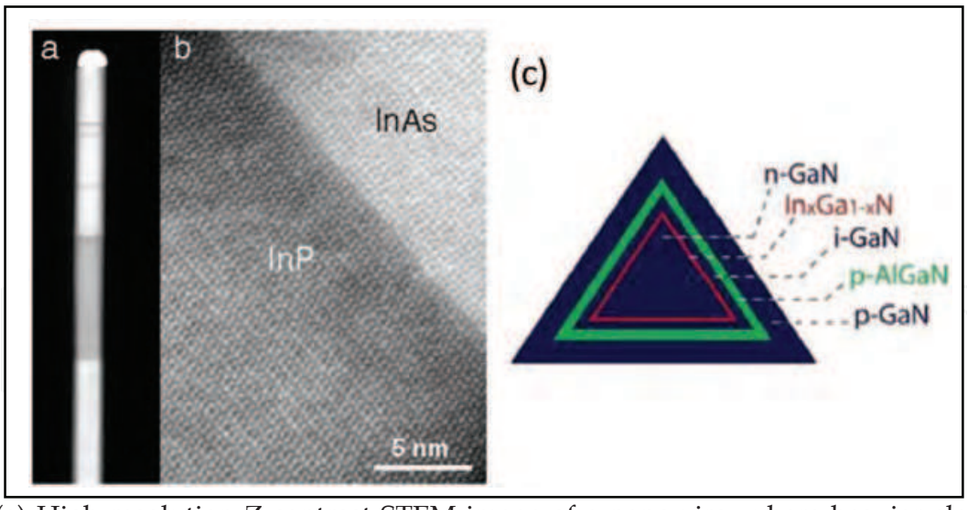

Fig. 9. (a) High resolution Z-contrast STEM image of a nanowire, where heavier elements, such as the gold particle at the top of the wire, show up brighter. The bright areas of the wire are InAs and the darker area is a 150 nm InP segment. (b) A high-resolution STEM image shows the atomically sharp interface, free from dislocations, between the InAs and the InP segments.[90] (c) Cross-sectional view of a core/multi-shell nanowire structure.[91]

Apart from large-area epitaxial films, even in the synthesis of nanometer-scale semiconductor structures, the use of single-crystal substrates as a starting platform is very common. For instance, epitaxial growth of semiconductor nanowires generally makes use of single-crystal substrates. In fact, the growth of group III-V compound semiconductor nanowires has been demonstrated almost exclusively on single-crystal substrates, including GaAs or InP nanowires grown either on single-crystal group III-V compound semiconductor substrates[99] or on single-crystal Si substrates.[99,100]

In the growth of semiconductor nanowires on single-crystal substrates, surfaces of single-crystal substrates provide epitaxial information (e.g., crystallographic symmetries and lattice constants, etc.) to "seeds" of nanowires in the early stage of the growth. A variety of growth mechanisms have been suggested for the growth of various types of nanowires.[89,101] In contrast to the growth of 3D islands (e.g., InAs on GaAs (100) surfaces), the growth of nanowires can be viewed as a significantly complicated process due partly to the mechanism that leads to quasi one-dimensional shapes resulted from the anisotropy in growth rate in two different directions (i.e., directions perpendicular and parallel to the long axis of a nanowire). Another feature contributing to various complications involved in the growth of nanowires is the presence of metal catalysts (e.g., metal-catalyzed nanowire growth with the presence of transition metal or noble metal particles).[102,103,104] Catalyst-free nanowire growths were also suggested,[105,106,107] however the level of complexities that would have to be handled in analyzing the growth of nanowires without metal-catalysts appears to be even much higher than that in metal-catalyzed nanowire growths. Therefore, the discussion on the role played by single-crystal substrates in the growth of nanowires, with or without metal catalysts, appears to be still in its infancy. However, it is conceivable that if an individual nanowire "sees" short-range atomic order within an area on the scale that is comparable to or moderately larger than the size of a nanowire itself in its early stage of evolution, an individual nanowire would not be able to tell whether it sits on a single-crystal substrate or a small crystallite present in a non-single-crystal substrate. Apparently the major difference between the two cases; nanowires grown on a single-crystal substrate and those grown on small crystallites in a non-single-crystal substrate, is that two different locations on the surface of a single-crystal substrate are correlated with its specific crystallographic translational operation whereas two different small crystallites that exist in a non-single-crystal substrate are not geometrically correlated, implying that, as long as geometrical synchronization or organization among a group of nanowires is not required, the use of a single-crystal substrate should not a required condition for the growth of nanowires.

In the following section, the idea of growing single-crystal group III-V compound semiconductor nanowires on various non-single-crystal substrates is reviewed. The structural concept of what is proposed is rather simple as schematically illustrated in Figs. 10(a)~(c). As postulated in Introduction, a starting substrate is non-single-crystal including amorphous and poly-crystal (note that there are a wide range of variations in this class of material, e.g., microcrystalline and nanocrystalline, etc.). Not constrained by the availability of appropriate single-crystal substrates, the freedom in choosing a starting substrate from a variety of materials will maximize flexibility in designing solid-state devices that utilize semiconductor nanowires. Although a non-single-crystal substrate can be chosen from such materials as glass or ceramics, one of the requirements that need to be carefully considered when a non-single-crystal substrate is selected is related to the fact that a non-single-crystal

substrate needs to withstand all succeeding process steps, in other words, a selected non-single-crystal substrate has to be physically and chemically stable at every process step towards the end of the fabrication process sequence necessary for solid-state devices that employ nanowires.

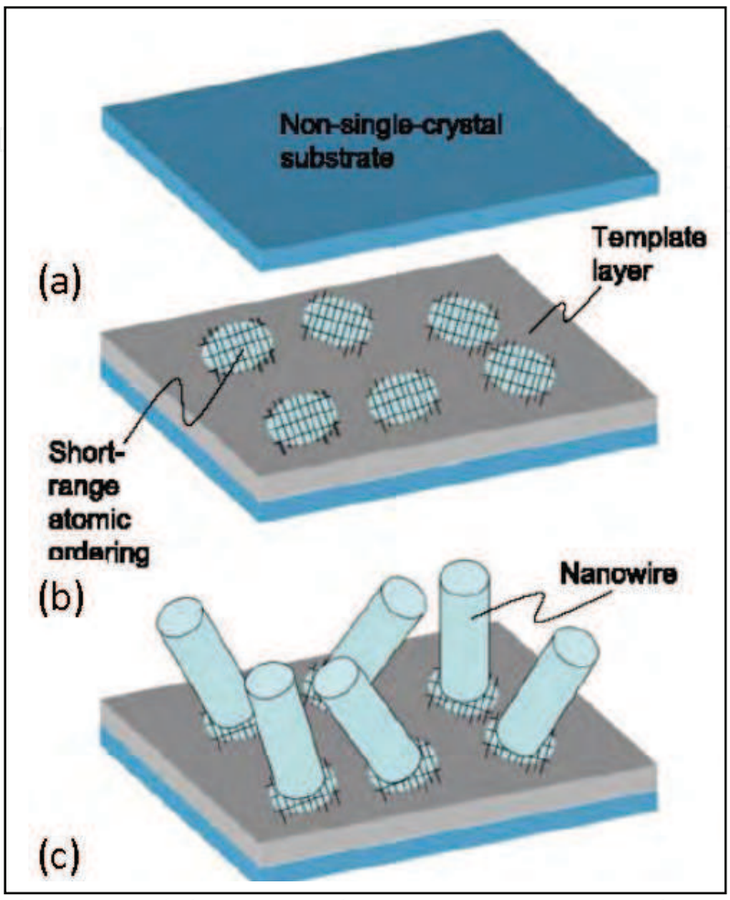

Fig. 10. Structural concept of the proposed route to grow semiconductor nanowires on a non-single-crystal substrate is schematically shown. A starting substrate in (a) can be chosen from various types of non-single-crystal including amorphous and poly-crystal. Once an appropriate non-single-crystal substrate is obtained, a template layer is prepared on the non-single-crystal substrate as in (b). The template layer can be made of a variety of materials as long as the template layer "locally" exhibits short-range atomic ordering on its surface. After nanowires are grown in (c), an ensemble of nanowires can be electrically accessible through the template layer.[109]

Amorphous silicon oxide (*a*-SiO_2) surfaces were used as a starting non-single-crystal substrate as shown in Fig. 10(a).[108] Subsequently, a template layer is prepared on the *a*-SiO_2 surface as in Fig. 10(b). The template layer can be made of a variety of materials as long as the template layer "locally" exhibits short-range atomic order on its surface. It is this short-range atomic order that is transferred to nanowires in the same sense as that in conventional epitaxial growth of a single-crystal thin film on a single-crystal substrate. As postulated earlier, it is short-range atomic order with a linear-scale comparable to or several times the diameter of nanowires that is critical for the formation of epitaxial single-crystal nanowires.

Although semiconductor single-crystal nanowires have been formed on non-single-crystal surfaces that were electrically insulating,[109,110,111] it is more advantageous, in specific applications as introduced later, to form an ensemble of single-crystal semiconductor nanowires with their one end electrically connected onto an electrically conductive template layer.

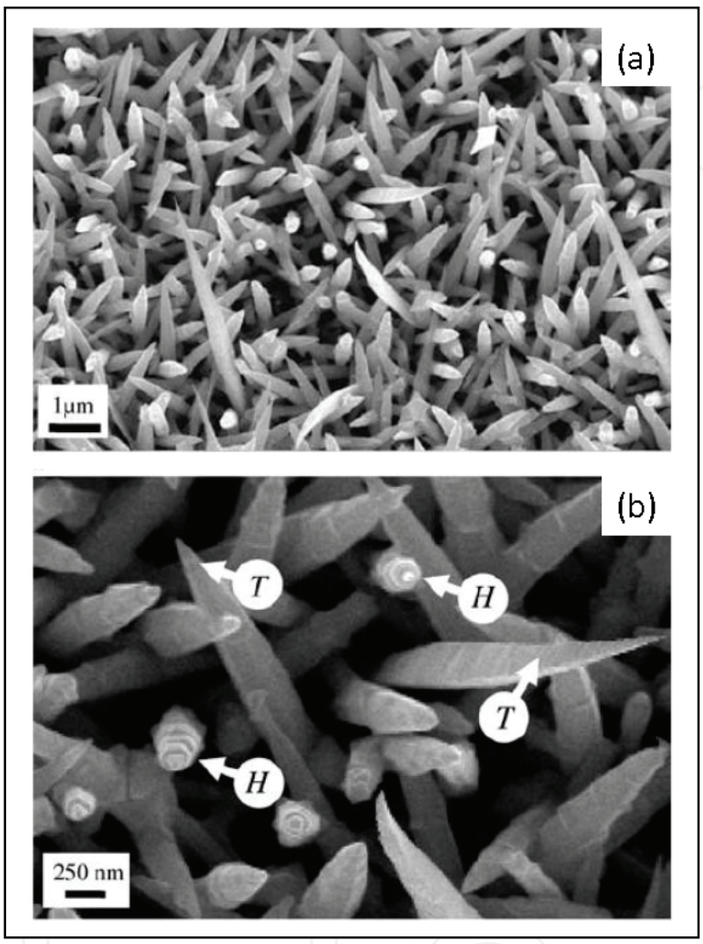

Fig. 11. Scanning electron microscope images of InP nanowires grown on a hydrogenated silicon surface. (a) top view at a low magnification, InP nanowires are randomly oriented with respect to the surface normal. (b) top view at a high magnification, the two types crystal habits are clearly seen.[112]

It is further advantageous if the electrical properties of a template layer are explicitly controlled so that an ensemble of nanowires is electrically accessed through an electrically conductive template layer as depicted in Fig. 10(c). This feature is, in fact, the one of two intriguing characteristics of our idea proposed here, that are; (1) epitaxial growth of semiconductor nanowires can be done on a non-single-crystal substrate by employing a template layer that possesses short-range atomic order and (2) an electrically conductive template layer establishes access to an ensemble of nanowires from external micrometer electrical circuits. In the selection of a material for the template layer, hydrogenated silicon (Si:H) was chosen for the demonstration of our idea because Si:H is essentially a

semiconductor that can be doped with a controlled manner to intentionally tune its electrical transport properties, which is significantly advantageous when solid-state devices that require *pn* junctions or Ohmic contacts are designed.

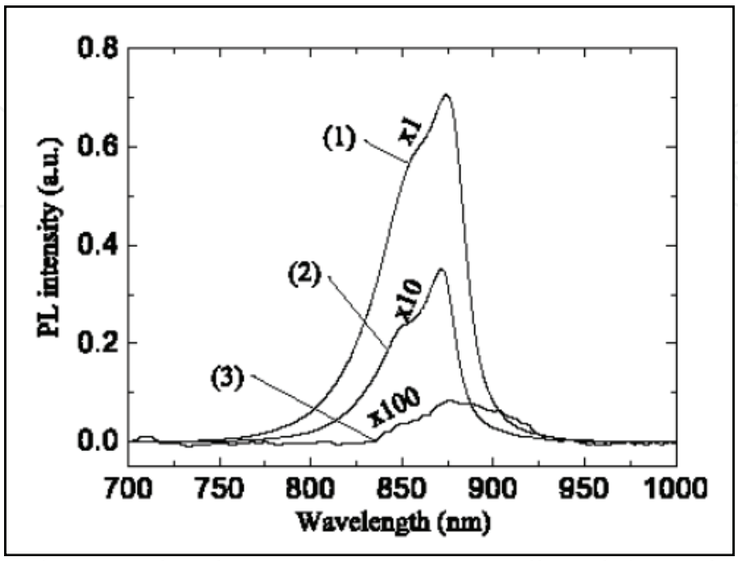

Fig. 12. A set of micro-photoluminescence spectra collected from the ensemble of InP nanowires at room temperature. The spectra (1)–(3) represent spectra collected from the InP nanowires on hydrogenated silicon at three different excitation power densities 6×103, 6×102and 6×101Wcm−2, respectively.[112]

Indium phosphide (InP) deposited with the presence of Au nanoparticles on the Si:H template layer prepared, as shown in Figs. 10, on the *a*-SiO_2 substrate was found to form nanowires. Fig. 11 is a scanning electron microscopy (SEM) image of the resulting InP nanowires. All nanowires appear to be randomly oriented as expected from the fact that the surface of the Si:H template layer on which the InP nanowires form is non-single-crystal. As seen in Fig. 11, two different crystal habits, some of which are marked with "*H*" and "*T*", were found in the ensemble of the nanowires. The nanowires denoted with *T* have a triangular cross section while the ones marked as *H* exhibit a hexagonal cross section. Since a specific crystal habit often reflects a unique crystallographic symmetry originated to that exists inside a single crystal, two different crystal habits seen in the SEM image suggest that there are two types of crystal structures co-existing in the ensemble of nanowires. The tapered feature of the both types of nanowires is clearly seen. Nominal geometrical dimensions of the two types of nanowires are summarized as; length is approximately 1.5~2 μm, lateral size at its bottom approximately 300~500 nm. The tapering angle of the nanowires (i.e., the angle between the long axis and side wall) is 33~39°. Analysis with transmission electron microscopy (TEM) revealed that the nanowires are single-crystal and there are two-types of crystal structures; zinc-blende (*ZB*) and wurtzite (*WZ*) co-existing within the ensemble of nanowires.[112] Photoluminescence studies shown in Fig. 12 suggest that the ensembles of InP nanowires are optically active.[113]

3.3 Building Blocks for Nanowire Solid-State Devices

Fabrication of robust electrical connections across nanowires is an essential step for implementing nanowires as an active part of solid-state devices. Electrical connections onto nanowires are also required to measure electrical transport properties of nanowires. Various techniques of contacting nanowires have been demonstrated by placing an individual nanowire across pre-fabricated metal electrodes on an insulating surface, or alternatively, placing an individual nanowire on an insulating surface and then, putting down a pair of electrodes onto the nanowire.[114,115] Apparently, these methods are not favorable to establishing reliable electrical contacts at large wafer scale. Nanowires bridging across a gap between semiconductor electrodes have also been demonstrated for silicon and III-V compound semiconductors,[116,117,118] in which single-crystal substrates were used. For certain applications, however the use of single-crystal substrates is not always desirable, which motivated us to develop the growth of group III-V compound semiconductor nanowires on non-single-crystal surfaces prepared on various substrates.

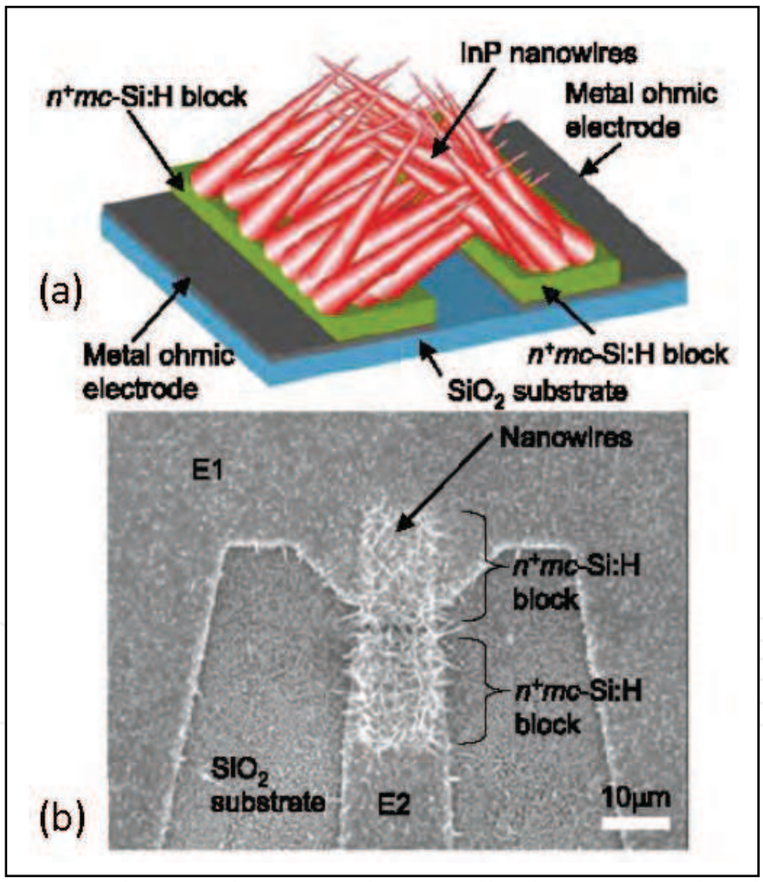

Fig. 13. InP nanowire photoconductor is schematically shown in (a) the planar structure in which InP nanowires can be selectively formed on *n+mc-Si:H surface offers great flexibility and simplification in building* devices that employ an ensemble of InP nanowires. Shown in (b) is an SEM top-view image collected on a representative InP nanowire photoconductor consisting of a pair of metal Ohmic electrodes (labeled E1 and E2) in a coplanar configuration that allows us to perform high speed testing.[109]

[112] Even for nanowires on non-single-crystal surfaces, electrical contacts still need to be made for device applications. In the following section, an ensemble of InP nanowires (InP NWs) that connect two planar hydrogenated silicon (Si:H) segments that serve as templates is described. The two Si:H segments are separated by a gap and bridged by having the InP NWs either be fused and/or grow directly across the gap. Photoelectric characteristics of an ensemble of InP NWs are presented with the view toward a wide range of optoelectronic solid-state devices. Two important features obtained by combining InP NWs with Si:H are (1) InP NWs maintain all the properties of a direct bandgap semiconductor and (2) thin film characteristics of Si:H provide not only a template for the catalytic growth of InP NWs but also electrical contacts to an ensemble of InP NWs. As shown in Fig. 13(a), an amorphous surface was prepared by growing a 2 μm thick silicon dioxide (SiO_2) on a 4 inch Si(100) substrate. After forming Pt/Ti electrodes onto the SiO_2 surface, a heavily doped *n*-type Si:H film (*n*+-Si:H) was deposited onto the patterned Pt/Ti electrodes. The *n*+-Si:H film was then patterned into two segments spatially separated and electrically isolated from each other. The processed wafer was then coated with Au nanoparticles. Finally, InP was deposited by low-pressure metal organic chemical vapor deposition on the processed wafer. InP grew into randomly oriented InP NWs formed selectively onto the *n*+-Si:H segments. The NWs bridged the gap by either fusing themselves or going across the gap. A planar structure in which InP NWs are selectively formed on *n*+-Si:H surface offers great flexibility and simplification in building solid-state devices that employ an ensemble of InP NWs. This planar structure (InP NW photoconducotor) was used to evaluate photoconductive properties of an ensemble of InP NWs. Shown in Fig. 13(b) is a scanning electron microscope image (top view) of the InP NW photoconductor on which a pair of electrodes (labeled E1 and E2) in a coplanar configuration is seen. A large number of randomly oriented nanowires are clearly seen on the two *n*+-Si:H segments. Detailed inspections by viewing the photoconductor from the side revealed that nanowires approaching from the two facing *n*+-Si:H segments collided and "fused" together in free space.

DC current-voltage (*IV)* characteristics of the InP NWs photoconductor were measured at room temperature.[119] Photoresponse was also obtained by illuminating the device with a laser at 633, 780, or 1550 nm. A 633 nm laser with various optical power densities in the range of 3~25 W/cm^2 (corresponding optical power of $6x10^{-7}$~$5x10^{-6}$ W) was used to illuminate the gap between the two *n*+-Si:H segments with InP NWs. As a control, the device prior to the InP NW growth was also evaluated. Prior to the InP NW growth, the measured photocurrent was <0.5 nA at all bias voltages with the highest illumination level, which was roughly three orders of magnitude smaller than those obtained from the device with InP NWs, suggesting the presence of negligible leak current in the reference sample without InP NWs. A semi-log plot in the inset of Fig. 14 shows the DC *IV* characteristics of the InP NW photoconductor obtained under different optical powers ($5x10^{-6}$ W for the top curve in black and no illumination for the bottom curve in dark green). The *IV* characteristics were remarkably symmetric with respect to 0 V and essentially Ohmic, revealing a clear contrast to nonlinear characteristics observed for nanowires in other configurations.[120] More than an order of magnitude increase in current at ±5 V, compared to that without illumination, was observed when the device was illuminated at $5x10^{-6}$ W. In the main plot of Fig. 14, a set of data points in different colors at a specific incident optical power represents resistivities of the InP NWs obtained at various bias voltages. As in a metal-semiconductor-metal photoconductor, the resistivity at a specific bias voltage

decreases as the incident optical power increases. The resistivity under the illumination at incident optical power >5x10^{-6} W seems to saturate, suggesting the resistivity is limited by the finite total volume provided by a limited number of nanowires available for the generation of excess electrons and holes. Unlike other nanowire-based photodetectors,[121] the photoconductor response presented above is insensitive to the polarization of the incident light, which is most likely due to the random orientation of the InP NWs. We believe that the arrangement of incorporating an ensemble of nanowires as an active part in solid-state devices presented in this study could be a new route to design solid-state devices that employ nanowires with highly anisotropic shapes.

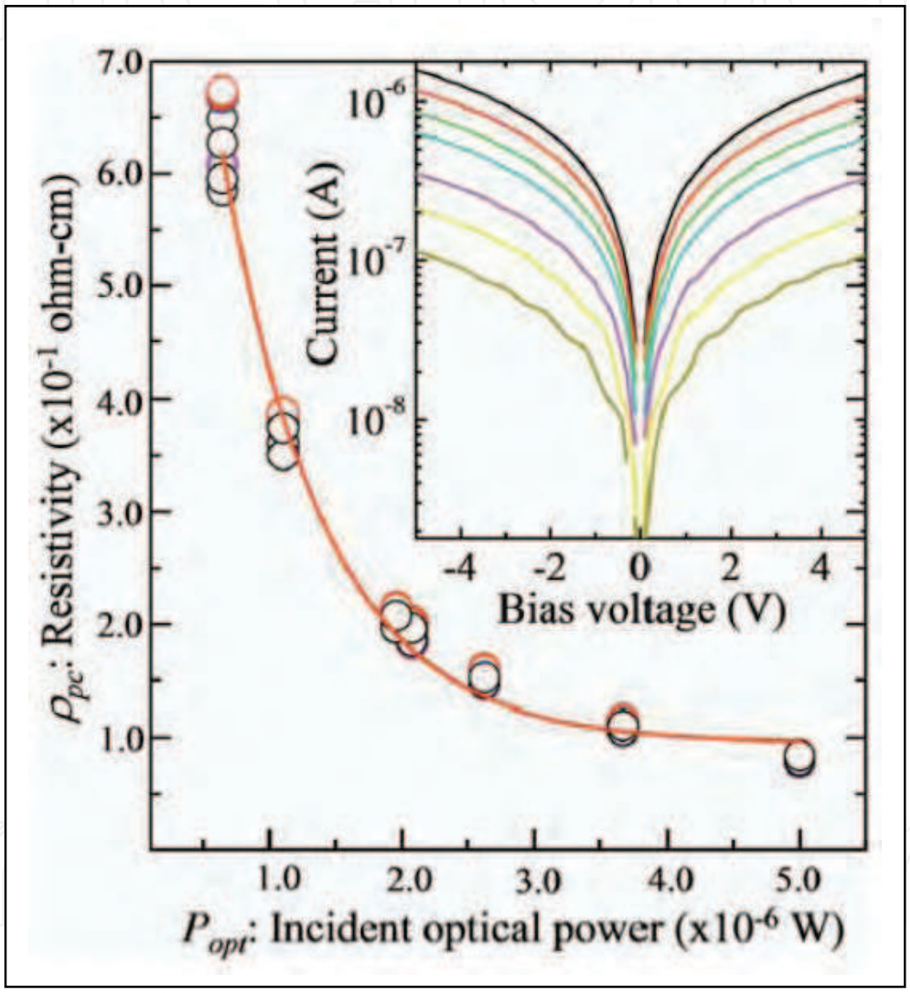

Fig. 14. Resistivities of the InP NWs are plotted as a function of the incident optical power by which the InP NW active region was illuminated. A set of data points in different colors at a specific incident optical power represents the resistivities obtained at different bias voltages ranging from −5 to 5 V with an increment of 1 V. Plotted in the inset are current-voltage characteristics collected under different levels of the incident optical power 5x10−6W for the top curve and 0 W for the bottom curve.119

4. Summary

InAs three-dimensional (3D) islands grown by molecular beam epitaxy on GaAs are described. The two-dimensional to three-dimensional morphological transition was studied with two complementary analytical techniques; scanning tunneling microscope and photoluminescence/photoluminescence excitation spectroscopy, to identify key features that exist at different stages of morphological evolution. The re-entrant behavior of small quasi-3D clusters existing prior to the appearance of 3D islands suggests that the quasi-3D clusters act as precursors of the 3D islands. Size evolution and vertical alignment of InAs 3D islands in a single and multiple stacks are illustrated. The lateral size and size dispersion were found to first increase drastically with a small amount of additional InAs deposition and then decrease and saturate, indicating the onset of a natural tendency for size equalization. The vertical alignment of multiple stacks of InAs 3D islands is a result of strain field generated by the 3D islands embedded within a GaAs matrix. All the insights we learned in the series of experiments would help us find a way to implement a group of 3D islands as a part of solid-state devices.

InP nanowires grown by metal organic chemical vapor deposition on non-single-crystal surfaces are described. Unlike conventional epitaxial thin films, the proposed route for growing nanowires requires no single-crystal surfaces. In principle, only short-range atomic order, in contrast to long-range atomic order required for the growth of epitaxial thin films, is necessary for nanowires. A template layer that possesses short-range atomic order prepared on a non-single-crystal surface is employed. Ensembles of InP nanowires were found to be single-crystal and electrically/optically active. DC electrical properties of simple photoconductors that employs an ensemble of InP nanowires were fabricated and characterized under light illumination. Our proposed path to implement semiconductor nanowires would unlock a path towards disruptive applications that require III–V compound semiconductors functionally integrated onto various material platforms.

5. Acknowledgement

I am grateful to many colleagues and peers in the course of gathering elemental building blocks for this chapter. Special thanks are due to Prof. A. Madhukar, Dr. Q. Xie, Dr. T. R. Ramachandran, Dr. R. Heitz, Dr. R. S. Williams, Dr. S.-Y. Wang, Prof. M. S. Islam, and Dr. Logeeswaran, V. J.

6. References

[1]Burton, W. K., Cabrera, N., Frank, F. C. (1951). The growth of crystals and the equilibrium structure of their surfaces, *Phil. Trans. Roy. Soc.* Vol. A234, pp. 299-358

[2]Gallet, F., Balibar, S., Rolley, E., Nozieres, P. (1987). The dynamic broadening of the roughening transition, *Japanese Journal of Applied Physics*, Sup. Vol. 26, pp. 389-90

[3]van der Merwe, J. H. (1993). Theoretical Considerations in Growing Uniform Epilayers, *Interface Science*, Vol. 1, pp. 77-86

[4] Venables, J. A. (1973). Rate equation approaches to thin film nucleation kinetics, *Philosophical Magazine,* Vol. 27, pp. 697-738

[5] Frankl, D. R., Venables, J. A. (1970). Nucleation on substrates from the vapour phase, *Advances in Physics*, Vol. 19, pp. 409-456

[6] Halpern, V. (1969). Cluster growth and saturation island densities in thin-film growth, *Journal of Applied Physics*, Vol. 40, pp. 4627-4636

[7] Joyce, B. A., Bradley, R. R., Booker, G. R. (1967), A study of nucleation in chemically grown epitaxial silicon films using molecular beam techniques. III. Nucleation rate measurements and the effect of oxygen on initial growth behavior, *Philosophical Magazine*, Vol. 15, pp. 1167-1187

[8]Lewis, B. (1971). Physical processes in epitaxial growth, *Thin Solid Films*, Vol. 7, pp. 179-217

[9]Stowell, M. J. (1972). Direct observations of epitaxial growth, *Thin Solid Films*, Vol. 12, pp. 341-54

[10]Stowell, M. J. (1970). Capture numbers in thin film nucleation theories, *Philosophical Magazine*, Vol. 26, pp. 349-60

[11]Zinsmeister, G. (1971). Theory of thin film condensation. IV. Influence of a variable collision factor, *Thin Solid Films*, Vol. 7, pp. 51-75

[12]Shockley, W., Read, W. T. (1949). Quantitative predictions from dislocation models of crystal grain boundaries, *Physical Review*, Vol. 75, pp. 692

[13]Read, W. T., Shockley, W. (1950). Dislocation models of crystal grain boundaries, *Physical Review*, Vol. 78, pp. 275-289

[14]van der Merwe, J. H. (1950). On the stresses and energies associated with inter-crystalline boundaries, *Proceedings of the Physical Society*, Vol. A63, pp. 616-637

[15]van der Merwe, J. H. (1962). Crystal interfaces. Part I. Semi-Infinite Crystals, *Journal of Applied Physics*, Vol. 34, pp. 117-122

[16]van der Merwe, J. H. (1963). Crystal interfaces. Part II. Finite overgrowths, *Journal of Applied Physics*, Vol. 34, pp. 123-127

[17]People, R., Bean, J. E. (1985). Calculation of critical layer thickness versus lattice mismatch for Ge_xSi_{1-x}/Si strained-layer heterostructures, *Applied Physics Letters*, Vol. 47, 322-324

[18] Matthews, J. W., Blakeslee, A. F. (1976). Defects in epitaxial multilayers III. Preparation of almost perfect multilayers, *Journal of Crystal Growth*, Vol. 32, pp. 265-273

[19]van der Merwe, J. H., Jesser, W.A. (1988). The prediction and confirmation of critical epitaxial parameters, *Journal of Applied Physics*, Vol. 64, pp. 4968-4974

[20]van der Merwe, J. H. (1970). Equilibrium structure of a thin epitaxial film, *Journal of Applied Physics*, Vol. 41, pp. 4725-4731

[21]Matthews, J. W. (1972). Influence of misfit dislocations on the alignment of epitaxial thin films, *Thin Solid Films*, Vol. 12, pp. 243-246

[22]Matthews, J. W., Blakeslee, A. E. (1974). Defects in epitaxial multilayers I. Misfit Dislocations, *Journal of Crystal Growth*, Vol. 27, pp. 118-125

[23]Matthews, J. W., Blakeslee, A. E. (1975). Defects in epitaxial multilatyers II. Dislocation pile-ups, threading dislocations, slip lines and cracks, *Journal of Crystal Growth*, Vol. 29, pp. 273-280

[24]Matthews, J. W., Blakeslee, A. E., Mader, S. (1976). Use of misfit strain to remove dislocations from epitaxial thin films, *Thin Solid Films*, Vol. 33, pp. 253-266

[25]Matthews, J. W., Jackson, D. C., Chambers, A. (1975). Effect of coherency strain and misfit dislocations on the mode of growth of thin films, *Thin Solid Films*, Vol. 26, pp. 129-134

[26]van der Merwe, J. H. (2001). Interfacial energy: bicrystals of semi-infinite crystals, *Progress in Surface Science*, Vol. 67, pp. 365-381

[27]Fletcher, N. H. (1964). Crystal interfaces, *Journal of Applied Physics*, Vol. 35, pp. 234-240

[28]Fletcher, N. H. (1967). Structure and energy of crystal interfaces II. A simple explicit calculation, *Philosophical Magazine*, Vol. 16, pp. 159-164

[29]Fletcher, N. H., Adamson, P. L. (1966). Structure and energy of crystal interfaces. I. Formal development, *Philosophical Magazine*, Vol. 14, pp. 99-110

[30]Tsao, J. Y., Dodson, B. W., Pieraux, S. T., Cornelson, D. M. (1987). Critical stresses for Si_xGe_{1-x} strained-layer plasticity, *Physical Review Letters*, Vol. 59, pp. 2455-2458

[31]Dodson, B. W., Tsao, J. Y. (1987). Relaxation of strained-layer semiconductor structures via plastic flow, *Applied Physics Letters*, Vol. 51, pp. 1325-1327

[32]Ghaisas, S. V., Madhukar, A. (1986). Role of Surface Molecular Reactions in Influencing the Growth Mechanism and the Nature of Non-Equilibrium Surfaces: A Monte-Carlo Study of Molecular Beam Epitaxy, *Physical Review Letters*, Vol. 56, pp.1066-1069

[33]Ghaisas, S. V., Madhukar, A. (1989). Kinetic Aspects of Growth Front Surface Morphology and Defect Formation During MBE Growth of Strained Thin Films, *Journal of Vacuum Science and Technology*, Vol. B7, pp. 264-268

[34]Ghaisas, S. V., Madhukar, A. (1988). Influence of compressive and tensile strain on growth mode during epitaxical growth: a computer simulation study, *Applied Physics Letters*, Vol. 53, pp. 1599-1601

[35]Arthur, J. R. (1974). Surface stoichiometry and structure of GaAs, *Surface Science*, Vol. 43, pp. 449-461

[36]Foxon, C. T., Joyce, B. A. (1975). Interaction kinetics of As_4 and Ga on {100} GaAs surfaces using a modulated molecular beam technique, *Surface Science*, Vol. 50, pp. 434-450

[37]Madhukar, A., Ghaisas, S. V. (1988). The nature of molecular beam epitaxial growth examined via computer simulations, *CRC Critical Reviews in Solid State and Materials Sciences*, Vol. 14, pp. 1-130

[38]Pashley, D. W. (1965). The nucleation, growth, structure and epitaxy of thin surface films, *Advances in Physics*, Vol. 14, pp. 327-410

[39]Matthews, J. W. (1972). Misfit dislocations and the alignment of epitaxial islands, *Surface Science*, Vol. 31, pp. 241-256

[40]van der Merwe, J. H., Bauer, E., (1989). Influence of misfit and bonding on the mode of growth in epitaxy, *Physical Review*, Vol. B39, pp. 3632-3641

[41]Stoop, L. C. A., van der Merwe, J. H. (1973). A simple model for layered growth in small epitaxial islands, *Thin Solid Films*, Vol. 17, pp. 291-309

[42]Shiramine, K., Muto, S., Shibayama, T., Sakaguchi, N., Ichinose, H., Kozaki, T., Sato, S., Nakata, Y., Yokoyama, N., Taniwaki, M. (2007). Tip artifact in atomic force microscopy observations of InAs quantum dots grown in Stranski–Krastanow mode, *Journal of Applied Physics*, Vol. 101, pp. 033527-5

[43]Bimberg, D., Grundmann, M., Ledentsov, N. N. (1988). Quantum Dot Heterostructures, John Willey & Sons, West Sussex, England

[44]Eaglesham, D. J. , Cerullo, M. (1990). Dislocation-free Stranski-Krastanow growth of Ge on Si(100), *Physical Review Letters*, Vol. 64, pp. 1943-1946

[45]Mo, Y.-W., Savage, D. E., Swartzentruber, B. S., Lagally, M. G., Kinetic pathway in Stranski-Krastanov growth of Ge on Si(001), *Modern Physics Letters B*, Vol. 4, pp. 1379-1384

[46]Guha, S., Madhukar, A., Rjkumar, K. C. (1990). Onset of incoherency and defect introduction in the initial stages of molecular beam epitaxial growth of highly strained $In_xGa_{1-x}As$ on GaAs(100), *Applied Physics Letters*, Vol. 57, pp. 2110-2112

[47]Houzay, F., Guille, C., Moison, J. M., Henoe, P., Barthe, F., (1987). First stages of the MBE growth of InAs on (001) GaAs, *Journal of Crystal Growth*, Vol. 81, pp. 67-72

[48]Lewis, B.F., Lee, T.C., Grunthaner, F.J., Madhukar, A., Fernandez, R., Maserjian, J. (1984). RHEED oscillation studies of MBE growth kinetics and lattice mismatch strain-induced effects during InGaAs growth on GaAs(100), *Journal of Vacuum Science & Technology B*, Vol. 2, pp. 419-424

[49]Snyder, C.W., Orr, B.G., Kessler, D., Sander, L. M. (1991). Effect of strain on surface morphology in highly strained InGaAs films, *Physical Review Letters*, Vol. 66, pp. 3032-3035

[50]Madhukar, A., Xie, Q., Chen, P., Konkar, A. (1994). Nature of strained InAs three-dimensional island formation and distribution on GaAs(100), *Applied Physics Letters*, Vol. 64, pp. 2727-2729

[51]Kobayashi, N. P., Ramachandran, T. R., Chen, P., Madhukar, A. (1996). In Situ atomic force microscope studies of the evolution of InAs three-dimensional islands on GaAs(001), *Applied Physics Letter*, Vol. 68, pp. 3299-3301

[52]Gerard, J.M., Genin, J.B., Lefebvre, J., Moison, J. M., Lebouche, N., Barthe, F. (1994). Optical investigation of the self-organized growth of InGaAs/GaAs quantum boxes, *Journal of Crystal Growth*, Vol. 150, pp. 351-356

[53]Leonard, D., Pond, K., Petroff, P. M. (1994). Critical layer thickness for self-assembled InAs islands on GaAs, *Physical Review B*, Vol. 50, pp. 11687-11692

[54]Polimeni, A., Patane, A., Capizzi, M., Martelli, F., Nasi, L., Salviati, G. (1996). Self-aggregation of quantum dots for very thin InAs layers grown on GaAs, *Physical Review B*, Vol. 53, pp. R4213-16

[55]Bressler-Hill, V., Lorke, A., Varma, S., Petroff, P. M., Pond, K., Weinberg, W. H. (1994). Initial stages of InAs epitaxy on vicinal GaAs(001)-(2*4), *Physical Review B*, Vol. 50, pp. 8479-8487

[56]Xie, Q., Madhukar, A., Chen, P., Kobayashi, N. P. (1995). Vertically self-organized InAs quantum box islands on GaAs(100), *Physical Review Letters*, Vol. 75, pp. 2542-2545

[57]Grundmann, M., Christen, J., Ledentsov, N. N., Bohrer, J., Bimberg, D., Ruvimov, S. S., Werner, P., Richter, U., Gosele, U., Heydenreich, J., Ustinov, V. M., Egorov, A. Yu., Zhukov, A. E., Kopev, P. S., Alferov, Zh. L. (1995). Ultranarrow luminescence lines from single quantum dots, *Physical Review Letters*, Vol. 74, pp. 4043-4046

[58]Xie, Q., Kalburge, A., Chen, P., Madhukar, A. (1996). Observation of lasing from vertically self-organized InAs three-dimensional island quantum boxes on GaAs (001), *IEEE Photonics Technology Letters*, Vol. 8, pp. 965-967

[59]Bimberg, D., Ledentsov, N. N., Grundmann, M., Kirstaedter, N., Schmidt, O. G., Mao, M. G., Ustinov, V. M., Egorov, A. Y., Zhukov, A. E., Kopev, P. S., Alferov, Zh. L. Ruvimov, S. Gosele, U., Heydenreich, J. (1996). InAs-GaAs quantum pyramid lasers: in situ growth, radiative lifetimes and polarization properties, *Japanese Journal of Applied Physics*, Part 1,Vol. 35, pp. 1311-1319

[60]Priester, C., Lannoo, M (1995). Origin of self-assembled quantum dots in highly mismatched heteroepitaxy, *Physical Review Letters*, Vol. 75, pp. 93-96

[61]Ramachandran, T. R., Heitz, R., Chen, P., Madhukar, A. (1996). Mass transfer in Stranski-Krastanow growth of InAs on GaAs, *Applied Physics Letters*, Vol. 70, pp. 640-642

[62]Ramachandran, T.R., Heitz, R., Kobyaahsi, N. P., Kalurge, A., Yu, W., Chen, P., Madhukar, A. (1997). Re-entrant behavior of 2D to 3D morphology change and 3D island lateral size equalization via mass exchange in Stranski-Krastanow growth: InAs on GaAs(001), *Journal of Crystal Growth*, Vol. 175/176, pp. 216-223

[63]Suekane, O., Hasegawa, S., Tanaka, M., Okui, T., Nakashima, H. (2002). Annealing effect on InAs islands on GaAs(001) substrates studied by scanning tunneling microscopy, *Applied Surface Science*, Vol. 190, pp. 218-221

[64] Lu, Z. D., Xu, J. Z., Zheng, B. Z., Xu, Z. Y., Ge, W. K. (1999). Effect of growth interruption on the optical properties of InAs/GaAs quantum dots, *Solid State Communications*, Vol. 109, pp. 649-653

[65]Patella, F., Arciprete, F., Placidi, E., Nufris, S., Fanfoni, M., Sgarlata, A., Schiumarini, D., Balzarotti, A., (2002). Morphological instabilities of the InAs/GaAs(001) interface and their effect on the self-assembling of InAs quantum-dot arrays, *Applied Physics Letters*, Vol. 81, pp. 2270-2272

[66]Schwoebel, R. L., Shipsey, E. J. (1966). Step Motion on Crystal Surfaces, *Journal of Applied Physics*, Vol. **37**, pp. 3682-3686

[67]Xie, Q., Chen, P., Kalburge, A., Ramachandran, T. R., Nayfonov, A., Konkar, A., Madhukar, A. (1995). Realization of optically active strained InAs island quantum boxes on GaAs(100) via molecular beam epitaxy and the role of island induced strain fields, *Journal of Crystal Growth*, Vol. 150, pp. 357-363

[68]Heitz, R., Ramachandran, T. R., Kalburge, A., Xie, Q., Mukhametzhanov, I., Chen, P., Madhukar, A. (1997). Obaservation of reentrant 2D to 3D morphology transition in highly strained epitaxy: InAs on GaAs, *Physical Review Letters*, Vol. 78, pp. 4071-4074

[69]Heitz, R., Grundmann, M., Ledentsov, N. N., Eckey, L., Veit, M., Bimberg, D., Ustinov, V. M., Egorov, A. Yu., Zhukov, A. E., Kop'ev, P. S., Alferov, Zh. I. (1996). Multiphonon-relaxation processes in self-organized InAs/GaAs quantum dots, *Applied Physics Letters*, Vol. 68, pp. 361-363

[70]Krzyzewski, T. J., Joyce, P. B., Bell, G. R., Jones, T. S. (2002). Role of two- and three-dimensional surface structures in InAs-GaAs(001) quantum dot nucleation, *Physical Review B*, Vol. 66, pp. 121307-1-4

[71]Costantini, G., Rastelli, A., Manzano, C., Acosta-Diaz, T. P., Katsaros, G., Songmuang, R., Schmidt, O. G., Knewl, O. V., Kern, K. (2005). Pyramids and domes in the InAs/GaAs(001) and Ge/Si(001) systems, *Journal of Crystal Growth*, Vol. 278, pp. 38-45

[72] Patella, Fl, Nufris, S., Arciprete, F., Fanfoni, M., Placidi, E., Sgarlata, Al., Blzarotti, A. (2003). Tracing the two- to three-dimensional transition in the InAs/GaAs(001) heteroepitaxial growth, *Physical Review B*, Vol. 67, pp. 205308-1-5

[73]Arciprete, F., Placidi, E., Sessi, V., Fanfoni, M., Patella, F., Balzarotti, A., Sessi, M., Fanfoni, F., Patella, Balzarotti, A. F., Arciprete, E., Placidi, V. (2006). How kinetics drives the two- to three-dimensional transition in semiconductor strained heterostructures: The case of InAs/GaAs(001), *Applied Physics Letters*, Vol. 89, pp. 041904 -1-3

[74]Heyn, Ch., Endler, D., Zhang, K., Hansen, W. (2000). Formation and dissolution of InAs quantum dots on GaAs, *Journal of Crystal Growth*, Vol. 210, pp. 421-428

[75]Drexler, H., Leonard, D., Hansen, W., Kotthaus, J. P., Petroff, P. M. (1994). Spectroscopy of quantum levels in charge-tunable InGaAs quantum dots, *Physical Review Letters*, Vol. 73, pp. 2252-2255

[76]Ponchet, A., LeCorre, A., L'Haridon, H., Lambert, B., Salaun, S. (1995). Relationship between self-organization and size of InAs islands on InP(001) grown by gas-source molecular beam epitaxy, *Applied Physics Letters*, Vol. 67, pp. 1850-1852

[77]Moison, J. M., Houzay, F., Barthe, F., Leprince, L., Andre, E., Vatel, O. (1994). Self-organized growth of regular nanometer-scale InAs dots on GaAs, *Applied Physics Letters*, Vol. 64, pp. 196-198

[78]Madhukar, A., Chen, P., Xie, Q., Konkar, A., Ramachandran, T. R., Kobayashi, N. P., Viswanathan, R. (1995). Low Dimensional Structures prepared by Epitaxial Growth or Regrowth on Patterned Substrates , *Proceedings of the NATO Advanced Workshop*, pp. 19-33, Ringberg Castle, Germany, February, 1995, The Netherlands

[79]Chen, P., Xie, Q., Madhukar, A., Chen, L., Konkar, A. (1994). Mechanisms of strained island formation in molecular-beam epitaxy of InAs on GaAs(100), *Journal of Vacuum Science & Technology B,* Vol. 12, pp. 2568-2573

[80]Gong, Q., Liang, J. B., Xu, B., Ding, D., Li, H. X., Jiang, C., Zhou, W., Liu, F. Q., Wang, Z. G., Qiu, X. H., Shang, G. Y., Bai, C. L. (1998). Analysis of atomic force microscopic results of InAs islands, *Journal of Crystal Growth*, Vol. 192, pp. 376-380

[81]Drucker, J. (1993). Coherent islands and microstructural evolution, *Physical Review B*, Vol. 48, pp. 18203-18206

[82]da Silvaa, M. J., Quivya, A. A., Gonz!alez-Borrerob, P. P., Marega Jr., E., Leitea, J. R. (2002). Atomic-force microscopy study of self-assembled InAs quantum dots along their complete evolution cycle, *Journal of Crystal Growth*, Vol. 241, pp. 19–30

[83]Jesson, D. E., Chen, G., Chen, K. M., Pennycook, S. J. (1998). Self-limiting growth of strained faceted islands, *Physical Review Letters*, Vol. 80, pp. 5156-5459

[84]Wang, L. G., Kratzer, P., Moll, N., Scheffler, M. (2000). Size, shape, and stability of InAs quantum dots on the GaAs(001) substrate, *Physical Review B*, Vol. 62, pp. 1897-1904

[85]Fafard, S., Leonard, D., Merz, J. L., Petroff, P. M. (1994). Selective excitation of the photoluminescence and the energy levels of ultrasmall InGaAs/GaAs quantum dots, *Applied Physics Letters*, Vol. 65, pp. 1388-1390

[86]Eisele, H., Lenz, A., Heitz, R., Timm, R., Dähne, M., Temko, Y., Suzuki, T., Jacobi, K. (2008). Change of InAs/GaAs quantum dot shape and composition during capping, *Journal of Applied Physics*, Vol. 104, pp. 124301-5

[87]Bouzaiene, L., Ilahi, B., Sfaxi, L., Hassen, F., Maaref, H., Marty, O., Dazord, J. (2004). Tuning vertically stacked InAs/GaAs quantum dot properties under spacer thickness effects for 1.3 μm emission, *Appl. Physics*, Vol., A79, pp. 587–591

[88]Heinrichsdorff, F., Mao, M. -H., Kirstaedter, N., Krost, A., Bimberg, D., Kosogovb, A. O., Werner, P. (1997). Room-temperature continuous-wave lasing from stacked InAs/GaAs quantum dots grown by metalorganic chemical vapor deposition, *Applied Physics Letters*, Vol. 71, pp. 22-24

[89]Wagner, R. S., Ellis, W. C. (1964), Vapor-liquid-solid mechanism of single crystal growth, *Applied Physics Letters*, Vol. 4, pp. 89-90

[90]Larsson, M. W., Wagner, J. B., Wallin, M., Hakansson, P., Froberg, L. E., Samuelson, L., Wallenberg, L. R. (2007). Strain mapping in free-standing heterostructured wurtzite InAs/InP nanowires, *Nanotechnology*, Vol. 18, pp. 015504-1-8

[91]Qian, F., Gradecak, S., Li, Y., Wen, C. –Y., Lieber C. M., (2005). Core/Multishell Nanowire Heterostructures as Multicolor, High-Efficiency Light-Emitting Diodes, *Nano Letters*, Vol. 5, pp. 11-2287-2291

[92]Persson, A. I., Larsson, M. W., Stenstrom, S., Ohlsson, B. J., Samuelson, L., Wallenberg, L. R. (2004). Solid-phase diffusion mechanism for GaAs nanowire growth, *Nature Materials*, Vol. 3, pp. 677-681

[93]Novotny, C. J., Yu, P. K. L. (2005). Vertically aligned, catalyst-free InP nanowires grown by metalorganic chemical vapor deposition, *Applied Physics Letters*, Vol. 87, pp. 203111-1-3

[94]Guichard, A. R., Barsic, D. N., Sharma, S., Kamins, T. I., Brongersma, M. L. (2006). Title: Tunable light emission from quantum-confined excitons in $TiSi_2$ -catalyzed silicon nanowires, *Nano Letters*, Vol. 6, pp. 2140-2144

[95]Dick, K. A. (2008). A review of nanowire growth promoted by alloys and non-alloying elements with emphasis on Au-assisted III-V nanowires, *Progress in Crystal Growth and Characterization of Materials*, Vol. 54, pp. 138-73 and references herein.

[96]Thelander, C., Agarwal, P., Brongersma, S. Thelander, C. Agarwal, P., Brongersma, S., Eymery, J., Feiner, L. F., Forchel, A., Scheffler, M., Riess, W., Ohlsson, B. J., Gösele, U., Samuelson, L. (2006). Nanowire-based one-dimensional electronics, *Materials Today*, Vol. 9, pp. 28-35

[97]Ertekin, E., Greaney, P.A., Chrzan, D.C., Sands, T. D. (2005). Equilibrium limits of coherency in strained nanowire heterostructures, *Journal of Applied Physics*, Vol. 97, pp. 114325-1-10

[98]Chuang, L. C., Moewe, M., Chase, C., Kobayashi, N. P., Chang-Hasnain, C., Crankshaw, S. (2007). Critical diameter for IIIVnanowires grown on lattice-mismatched substrates, *Applied Physics Letters*, Vol. 90, pp. 043115-1-3

[99]Yazawa, M., Koguchi, M., Hirutna, K. (1991). Heteroepitaxial ultrafine wire-like growth of InAs am GaAs substrates, *Applied Physics Letters*, Vol. 58, pp. 1080-1082

[100]Mårtensson, T., Patrik C., Svensson, T., Wacaser, B. A., Larsson, M. W., Seifert, W., Deppert, K., Gustafsson, A., Wallenberg, L. R., Samuelson, L. (2004). Epitaxial III-V Nanowires on Silicon, *Nano Letters*, Vol. 4, pp. 1987-1990

[101] Persson, A. I., Ohlsson, B. J., Jeppesen, S., Samuelson, L. (2004). Growth mechanisms for GaAs nanowires grown in CBE, Journal of Crystal Growth, Vol. 272, pp. 167-174

[102]Paiano, P., Prete, P., Loverginea, N., Mancini, A. M. (2006). Size and shape control of GaAs nanowires grown by metalorganic vapor phase epitaxy using tertiarybutylarsine, *Journal of Applied Physics*, Vol. 100, pp. 094305-1-4

[103]Kamins, T. I., Sharma, S., Yasseri, A. A., Li, Z., Straznicky, J. (2006). Metal-catalysed, bridging nanowires as vapor sensors and concept for their use in a sensor system, *Nanotechnology*, Vol. 17, pp. s291-297

[104]Sko1ld, N., Karlsson, L. S., Larsson, M. W., Pistol, M. –E., Seifert, W., Trägårdh, J., Samuelson, L. (2005). Growth and optical properties of strained GaAs-GaxIn1-xP core-shell nanowires, *Nano Letters*, Vol. 5, pp. 1943-1947

[105]Novotny, C. J., Yu, P. K. L. (2005). Vertically aligned, catalyst-free InP nanowires grown by metalorganic chemical vapor deposition, *Applied Physics Letters*, Vol. 87, pp. 203111-1-3

[106]Mattila, M., Hakkarainen, T., Lipsanen, H., Jiang, H., Kauppinen, E. I. (2006). Catalyst-free growth of In(As)P nanowires on silicon, *Applied Physics Letters*, Vol. 89, pp. 063119-1-3

[107]Noborisaka, J., Motohisa, J., Fukui, T. (2005). Catalyst-free growth of GaAs nanowires by selective-area metalorganic vapor-phase epitaxy, *Applied Physics Letters*, Vol. 86, pp. 213102-1-3

[108]Kobayashi, N. P., Mathai, S., Li, X., Logeeswaran, V. J., Islam, M. S., Lohn, A., Onishi, T., Stranznicky, J., Wang, S. –Y., Williams, R. S. (2009). Ensembles of indium phosphide nanowires: physical properties and functional devices integrated on non-single crystal platforms, *Applied Physics A*, Vol. 95, pp. 1005-1013.

[109]Gudiksen, M. S., Wang, J., Lieber, C. M. (2002). Size-Dependent Photoluminescence from Single Indium Phosphide Nanowires, *Journal of Physical Chemistry B*, Vol. 106, pp. 4036-9

[110]Vaddiraju, S., Mohite, A., Chin, A., Meyyappan, M., Sumanasekera, G., Alphenaar, B. W., Sunkara, M. K. (2005). Mechanisms of 1D Crystal Growth in Reactive Vapor Transport: Indium Nitride Nanowires, *Nano Letters*, Vol. 5, pp. 1625-1631

[111]Gao, P. X., Lao, C. S., Hughes, W. L., Wang, Z. L. (2005). Three-dimensional interconnected nanowire networks of ZnO, *Chemical Physics Letters*, Vol. 408, pp. 174-178

[112]Kobayashi, N.P., Wang, S.-Y., Santori, C., Williams, R. S. (2006) Growth and characterization of indium phosphide single-crystal nanoneedles on microcrystalline silicon surfaces, *Applied Physics A*, Vol. A85, pp. 1-6

[113]Kobayashi, N.P., Shih-Yuan Wang, Santori, C., Williams, R. S. (2007). Indium phosphide nanoneedles on non-single crystalline semiconductor surfaces, *Japanese Journal of Applied Physics*, Part 1, Vol. 46, pp. 6346-6351

[114]Pettersson, H., Tragardh, J., Persson, A.I., Landin, L., Hessman, D., Samuelson, L. (2006). Infrared photodetectors in heterostructure nanowires , *Nano Letters*, Vol. 6, pp. 229-232

[115]Salfi, J., Philipose, U., de Sousa, C. F., Aouba, S., Ruda, H. E. (2006). Electrical properties of Ohmic contacts to ZnSe nanowires and their application to nanowire-based photodetection, *Applied Physics Letters*, Vol. 89, pp. 261112-1-3

[116]Haraguchi, K., Hiruma, K., Katsuyama, T., Tominaga, K., Shirai, M., Shimada, T. (1996). Self-organized fabrication of planar GaAs nanowhisker arrays, *Applied Physics Letters*, Vol. 69, pp. 386-387

[117]Islam, M.S., Sharma, S. , Kamins, T. I., Williams, R. S. (2004). Ultrahigh-density silicon nanobridges formed between two vertical silicon surfaces, *Nanotechnology*, Vol. 15, pp. L5-8

[118]Yi, S. S., Girolami, G., Amano, J., Islam, M. S., Sharma, S., Kamins, T. I. (2006). InP nanobridges epitaxially formed between two vertical Si surfaces by metal-catalyzed chemical vapor deposition, *Applied Physics Letters*, Vol. 89, pp. 133121-1-3

[119]Kobayashi, N. P., Logeeswaran, V. J., Islam, M. S., Li, X., Straznicky, J. ,Wang, S. –Y., Williams, R. S., Chen, Y. (2007). Hydrogenated microcrystalline silicon electrodes connected by indium phosphide nanowires, *Applied Physics Letters*, Vol. 91, pp. 113116-1-3

[120]Law, J. B. K., Thong, J. T. L. (2006). Simple fabrication of a ZnO nanowire photodetector with a fast photoresponse time, *Applied Physics Letters*, Vol. 88, pp. 133114-1-3

[121]Hayden, O., Agarwal, R., Lieber, C. M. (2006). Nanoscale avalanche photodiodes for highly sensitive and spatially resolved photon detection, *Nature Materials*, Vol. 5, pp. 352-356

Cutting Edge Nanotechnology

Edited by Dragica Vasileska

ISBN 978-953-7619-93-0
Hard cover, 444 pages
Publisher InTech
Published online 01, March, 2010
Published in print edition March, 2010

The main purpose of this book is to describe important issues in various types of devices ranging from conventional transistors (opening chapters of the book) to molecular electronic devices whose fabrication and operation is discussed in the last few chapters of the book. As such, this book can serve as a guide for identifications of important areas of research in micro, nano and molecular electronics. We deeply acknowledge valuable contributions that each of the authors made in writing these excellent chapters.

How to reference

In order to correctly reference this scholarly work, feel free to copy and paste the following:

Nobuhiko P. Kobayashi (2010). Low-Dimensional Group III-V Compound Semiconductor Structures, Cutting Edge Nanotechnology, Dragica Vasileska (Ed.), ISBN: 978-953-7619-93-0, InTech, Available from: http://www.intechopen.com/books/cutting-edge-nanotechnology/low-dimensional-group-iii-v-compound-semiconductor-structures

INTECH
open science | open minds

InTech Europe
University Campus STeP Ri
Slavka Krautzeka 83/A
51000 Rijeka, Croatia
Phone: +385 (51) 770 447
Fax: +385 (51) 686 166
www.intechopen.com

InTech China
Unit 405, Office Block, Hotel Equatorial Shanghai
No.65, Yan An Road (West), Shanghai, 200040, China
中国上海市延安西路65号上海国际贵都大饭店办公楼405单元
Phone: +86-21-62489820
Fax: +86-21-62489821

IntechOpen